Available online at www.sciencedirect.com
SCIENCE DIRECT®
Mechanics of Materials 36 (2004) 975–997
MECHANICS OF MATERIALS
www.elsevier.com/locate/mechmat

Micromagnetic modeling of magnetostrictive materials under intrinsic stress

Y.C. Shu *, M.P. Lin, K.C. Wu

Institute of Applied Mechanics, National Taiwan University, Taipei 106, Taiwan, ROC

Received 16 September 2002; received in revised form 25 March 2003

Abstract

We have developed a framework based on micromagnetics to explore the effect of stress on the magnetostrictive behavior in ferromagnetics. Our approach is different from the conventional one which simply replaces the total strain by magnetostrain. Question arises for such an approach because of the loss of strain compatibility. Here, we have included the kinematic constraints in our micromagnetic model and developed a modified boundary integral formalism to calculate the intrinsic stress induced by incompatible magnetostrain. We have shown that for small magnetostriction of the order of 10^{-5}, the results predicted by the present approach are slightly different from those predicted by the conventional method. But we have found that for large magnetostriction around 10^{-3} order of magnitude, the conventional approach is insufficient to predict magnetic domain patterns and hysteresis precisely, and the effective magnetic field induced by intrinsic stress cannot be neglected.

Keywords: Incompatible magnetostrain; Micromagnetics; Magnetostriction

1. Introduction

A magnetostrictive material is one which is able to change its physical dimensions in response to a change of state of magnetization. In other words, it exhibits a change in length accompanied by an inverse change in girth when it is subjected to a magnetic field. Conversely, the state of magnetization changes if an external force is applied causing strain. The coupling between magnetic and mechanical energies gives rise to the capability in transduction that allows a magnetostrictive material to be used in actuator and sensor applications. All ferromagnetic materials exhibit varying degrees of magnetostrictive strain, however only some of them exhibit sufficient strain for practical use. The highest room temperature magnetostrictive strain of a pure element is that of Co which is extremely small and is around 60 microstrain at saturation. Fe and Ni are common ferromagnetic materials and also have magnetostriction with magnitudes around this range. On the other hand, by alloying elements "giant" magnetostriction under relatively small magnetic fields can be achieved (Clark, 1980). Among these, Terfenol-D ($Tb_xDy_{1-x}Fe_2$, $x \approx 0.3$) is at present the most widely used magnetostrictive material. It

* Corresponding author. Tel.: +886-2-3366-5627; fax: +886-2-2363-9290.
E-mail address: yichung@spring.iam.ntu.edu.tw (Y.C. Shu).

0167-6636/$ - see front matter © 2003 Elsevier Ltd. All rights reserved.
doi:10.1016/j.mechmat.2003.04.004

is capable of strains as high as 1600 microstrain and, since the 1980s, has enjoyed the greatest commercial success for application in a great many fields (Jiles, 1994).

Magnetostrictive materials at no applied fields often display extremely complex domains on which magnetization and strain are approximately constant. These domains, occurring at a microscopic scale, evolve under the action of applied fields and loads which in turn give rise to the overall response of the materials. Therefore, studying the mechanism that governs domain evolution is a key step toward understanding the macroscopic behavior of magnetostrictive materials. In the past several decades domain analysis and evolution under external fields have been studied extensively for rigid ferromagnetic materials within the framework of micromagnetic theory developed by Brown (1963) and his followers (see Aharoni, 1996 for an extensive review and James and Kinderlehrer, 1990 for a modern treatment). In spite of many useful results predicted by this theory, very few analytic solutions of Brown's micromagnetic equations have been found in literature as these equations are inherently nonlinear and nonlocal in nature. Numerical micromagnetics, on the other hand, provides an alternative to apply micromagnetic methods to large-scale domain structures. Nowadays computational micromagnetics has led to a deeper understanding of hysteresis behavior by visualization of magnetization reversal (Fidler and Schrefl, 2000).

Complicated magnetomechanical coupling and time consuming computation, however, have prevented many useful methods proposed originally for rigid ferromagnetics from being applied directly to deformable ferromagnetics. Much has been done for theoretical development of magnetostrictive materials. It includes early pioneering works such as Brown (1966), Tiersten (1965), Pao and Yeh (1973), Hutter and van de Ven (1978) and Jiles and Atherton (1984) (see also Eringen and Maugin, 1990; Maugin, 1988 and references therein). James and Kinderlehrer (1993) and DeSimone and James (2002) have proposed an energetic approach and used very sophisticated modern mathematical techniques to analyze domains in giant magnetostrictive materials. However, little or none has provided a convenient way for direct simulation of domain patterns and evolution under external fields and loads for a wide class of magnetostrictive materials. Fabian and Heider (1996) have used the continuum theory of defects to include magnetostriction in micromagnetic calculation with some success in studying titanomagnetites. Recently Voltairas et al. (2000a,b) have studied nonuniform magnetization reversal in stressed ferromagnetic films. Their simulation of magnetization reversal, however, is confined to be one-dimensional with severe restrictions on elastic states.

To overcome difficulties in the calculation of magnetostrictive energy, the conventional approach to include magnetostriction is to replace the total compatible strain by magnetostrictive strain in micromagnetic models (Cullity, 1972; Zhu, 1993; Callegaro and Puppin, 1997). As a consequence, the energy of applied loads becomes another source of magnetic anisotropy energy while the magnetostrictive self-energy vanishes. The intrinsic stress resulting from incompatible magnetostrictive strain as magnetization rotates is not taken into account while the external stress causes the induction of a magnetostrictive uniaxial anisotropy, usually called *stress-induced anisotropy* (Izawa, 1984; Jeong and Bogy, 1995). The material is then treated as a rigid ferromagnetics with varying magnetic easy axes depending on external stress. Recently Zhu et al. (2001) have used this approach to study the influence of external stress on coercivity in magnetic thin films and obtained qualitatively general agreement with experiment (Callegaro and Puppin, 1996). Although the results obtained by this approximation have been found to be useful in various applications, question arises because of loss of strain compatibility and negligence of intrinsic stress. This paper is primarily concerned with this issue and studies the effect of intrinsic stress on the magnetostrictive behavior in various ferromagnetic materials. In addition, a new method for the direct simulation of magnetic domains and their evolution under external fields and loads is proposed here.

Our framework is based on micromagnetics accounting for magnetostrictive effect. Micromagnetics is a nonlocal, nonconvex variational

problem. We write in Section 2 the total energy of the crystal as a sum of the exchange energy between the spins, the total anisotropy energies including magnetostrictive energy, the energy of the applied fields and loads, and the energy of the induced magnetic field. The state of the ferromagnetic crystal is obtained as minimizers of this total energy subject to two constrained equations: Maxwell's and elastic equilibrium equations. The anisotropy energy density encodes phenomenologically the information that the crystal prefers certain magnetized and distorted states, and can be nonconvex with multiple wells due to the presence of multiple such states. It can be shown that energy minimization based on this theory automatically leads to domain patterns in equilibrium based on very few parameters (James and Kinderlehrer, 1993; James and Wuttig, 1998). Instead of providing further mathematical analysis on magnetic domains, we study the solutions of micromagnetic equations deduced from the present theory. We use the Landau–Lifshitz–Gilbert (LLG) equation to obtain both equilibrium and transient magnetization configurations. The LLG equation is derived based on the microscopic physics and is able to describe the relaxation process of the magnetization. We emphasize this point by showing in Section 2.4 that the total free energy is decreasing as magnetization evolves under the LLG equation.

The key issue in performing simulation of domain evolution is to solve the elastic equilibrium equation for each magnetization configuration. This method, which we call the *constrained approach* here, is in contrast to the *relaxed approach* that neglects the effect of intrinsic stress. In Section 3, we calculate the magnetostrictive energy which requires the solution of a boundary value problem in elasticity theory. Since such a calculation has to be performed at every step of the iterative procedure, a time consuming computation seems to be inevitable. Fortunately, the improved availability of large-scale computer power has enabled us to include magnetostrictive effect in the LLG solver and provides us an opportunity for deeper understanding of detailed and subtle physical behavior of magnetization reversal. As the stress-induced magnetic field (see (2.14)) involves variable strain rather than displacement, we develop a strain-based boundary integral formulation in Section 3.3. This formalism, originally proposed by Wu et al. (1992), has been shown to be more accurate in the calculation of stress as well as have faster rate of convergence than conventional displacement-based numerical schemes. We extend their formulation to account for the effect of magnetostrictive stress and implement the associated numerical algorithm in Section 4.

The simulation results for various magnetostrictive films are presented in Section 5. We study magnetization in equilibrium and reversal using constrained and relaxed methods and make comparison between these two approaches. We use Ni and Terfenol-D as the model materials to represent for ferromagnetics with small and large magnetostrictive strains, respectively. Our simulation demonstrates that the relaxed approach turns out to be a reasonable approximation in predicting equilibrium domains and their evolution in Ni films while it becomes a crude estimation for Terfenol-D films. It shows that the effective magnetic field induced by intrinsic stress cannot be ignored for materials with large magnetostrictive strain. We conclude in Section 6 with a discussion.

2. Framework and formulation

2.1. Kinematics and magnetostriction

Magnetostriction is the spontaneous deformation of a magnetic crystal caused by a change of its state of magnetization. Certain materials such as Ni_2MnGa, one of ferromagnetic shape-memory materials, have extremely large magnetostriction of the order of 10^{-1} (Ullakko et al., 1996; Tickle and James, 1999; Wu et al., 2002). They are not taken into account here because of difficulty in handling physical quantities defined in deformed configuration. We refer to James and Kinderlehrer (1993) and James (2002) for detailed discussion. Instead, materials under consideration here such as Fe, Ni or Terfenol-D have magnetostriction with orders ranging from 10^{-3} to 10^{-5}. Such a small change in shape suggests us to choose the geometrically linear framework of micromagnetics, which Brown has called the conventional theory of magnetostriction

(Brown, 1966). However, we are aware that, as pointed out by Brown (1966), this conventional linear strain formulation misses certain terms that should be present according to a direct linearization starting from the geometrically nonlinear theory. As a result, the magnetic body force and body couple are neglected, and the anti-symmetric part of stress vanishes. With these reservations, we consider a ferromagnetic single crystal shown in Fig. 1. The crystal occupies the region $\Omega \subset \mathbb{R}^3$ in its reference configuration. The displacement of the crystal is described by the function $\mathbf{u} : \Omega \to \mathbb{R}^3$ and the linear strain is denoted by $\boldsymbol{\varepsilon} : \Omega \to \mathbb{M}_s^{3\times 3}$ where $\mathbb{M}_s^{m\times m}$ is the set of all symmetric second-order tensors defined in $\mathbb{R}^m$. The displacement–strain relation is given by

$$\boldsymbol{\varepsilon}[\mathbf{u}] = \frac{1}{2}\left\{\nabla\mathbf{u} + (\nabla\mathbf{u})^{\mathrm{T}}\right\}. \tag{2.1}$$

The conventional theory of ferromagnetics assumes that below the Curie temperature the magnetization $\mathbf{M}$ varies with point $\mathbf{x}$ in Ω while maintaining a fixed magnitude:

$$|\mathbf{M}(\mathbf{x})| = M_s \quad \forall \mathbf{x} \in \Omega, \tag{2.2}$$

where M_s is called the *saturation magnetization* which is a material constant depending on temperature only. Let

$$\mathbf{m}(\mathbf{x}) = \frac{1}{M_s}\mathbf{M}(\mathbf{x}) : \Omega \to S^2, \tag{2.3}$$

where S^2 denotes the three-dimensional sphere of unit radius. The free or spontaneous *magnetostrain tensor* corresponding to the magnetization $\mathbf{m}$ is denoted as $\boldsymbol{\varepsilon}^0(\mathbf{m}) : \Omega \to \mathbb{M}_s^{3\times 3}$. In the case of cubic materials the most general quadratic form of $\boldsymbol{\varepsilon}^0(\mathbf{m})$ is

$$\boldsymbol{\varepsilon}^0(\mathbf{m}) = \frac{3}{2}\left\{\lambda_{100}\left(\mathbf{m}\otimes\mathbf{m} - \frac{1}{3}\mathbf{I}\right) + (\lambda_{111} - \lambda_{100})\sum_{i\neq j} m_i^{\mathrm{c}} m_j^{\mathrm{c}} (\mathbf{e}_i^{\mathrm{c}} \otimes \mathbf{e}_j^{\mathrm{c}})\right\}, \tag{2.4}$$

where $\mathbf{I} \in \mathbb{M}_s^{3\times 3}$ is the identity tensor, $\{\mathbf{e}_1^{\mathrm{c}}, \mathbf{e}_2^{\mathrm{c}}, \mathbf{e}_3^{\mathrm{c}}\}$ is an orthonormal set of crystal basis, m_i^{c} are components of $\mathbf{m}$ in the crystal basis, λ_{100} and λ_{111} are independent, dimensionless material parameters indicating the strength of the magnetoelastic interaction. Above $\mathbf{a}\otimes\mathbf{b}$ is the tensor product of two vectors $\mathbf{a}$ and $\mathbf{b}$ with components $(\mathbf{a}\otimes\mathbf{b})_{ij} = a_i b_j$ in some orthonormal basis. Note that magnetostrain $\boldsymbol{\varepsilon}^0(\mathbf{m})$ is an even function in $\mathbf{m}$; i.e., $\boldsymbol{\varepsilon}^0(\mathbf{m}) = \boldsymbol{\varepsilon}^0(-\mathbf{m})$.

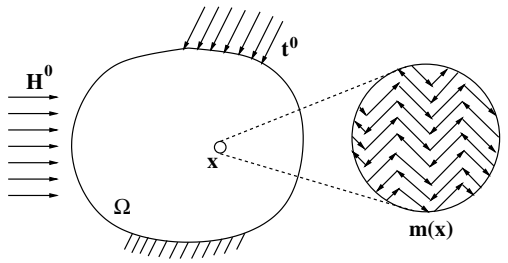

Fig. 1. A ferromagnetic crystal subjected to external magnetic field $\mathbf{H}^0$ and mechanical loading $\mathbf{t}^0$.

2.2. Magnetoelastic energy

Let $\partial\Omega$ denote the boundary of the domain Ω and $\chi_\Omega(\mathbf{x})$ the characteristic function of Ω such that $\chi_\Omega = 1$ in Ω and $\chi_\Omega = 0$ outside Ω. Assume $\partial\Omega = \partial\Omega_1 \cup \partial\Omega_2 \cup \partial\Omega_3$ where $\partial\Omega_i \cap \partial\Omega_j = \emptyset$ a.e. for $i \neq j$. Let $\mathbf{u}^0 : \partial\Omega_1 \cup \partial\Omega_3 \to \mathbb{R}^3$ and $\mathbf{t}^0 : \partial\Omega_2 \cup \partial\Omega_3 \to \mathbb{R}^3$ be the applied displacement and traction on the boundary $\partial\Omega$. The mechanical boundary conditions are for $i, j = 1, 2, 3$,

$$\begin{aligned} &\mathbf{u} = \mathbf{u}^0, \quad \mathbf{x} \in \partial\Omega_1, \\ &\boldsymbol{\sigma}\mathbf{n} = \mathbf{t}^0, \quad \mathbf{x} \in \partial\Omega_2, \\ &\mathbf{u}\cdot\mathbf{l}_i = u_i^0, \ \ (\boldsymbol{\sigma}\mathbf{n})\cdot\mathbf{l}_j = t_j^0, \ \ i \neq j, \quad \mathbf{x} \in \partial\Omega_3, \end{aligned} \tag{2.5}$$

where $\boldsymbol{\sigma} : \Omega \to \mathbb{M}_s^{3\times 3}$ is the stress tensor and $\{\mathbf{l}_1, \mathbf{l}_2, \mathbf{l}_3\}$ is an orthonormal set of vectors such that $\mathbf{l}_1$ and $\mathbf{l}_2$ are tangent to the boundary $\partial\Omega_3$ and $\mathbf{l}_3 = \mathbf{n}$ is the unit outward normal to the boundary $\partial\Omega_3$. Note that the boundary condition $(2.5)_3$ is the mixed type and $\mathbf{u}^0 \cdot \mathbf{t}^0 = 0$ there. Let $\mathbf{H}^0 : \mathbb{R}^3 \to \mathbb{R}^3$ be the applied magnetic field that would be present were the ferromagnetic crystal absent.

We postulate that below the Curie point we can obtain the magnetization as the one that minimizes

$$\mathscr{E}(\mathbf{m}) = \int_\Omega \Big\{ \nabla\mathbf{m}\cdot\mathbf{A}\nabla\mathbf{m} + W_{\mathrm{a}}(\mathbf{m}) + \frac{1}{2}\big[\boldsymbol{\varepsilon}-\boldsymbol{\varepsilon}^0(\mathbf{m})\big]\cdot\mathbf{C}\big[\boldsymbol{\varepsilon}-\boldsymbol{\varepsilon}^0(\mathbf{m})\big]\Big\}\mathrm{d}\mathbf{x} - \int_\Omega \mu_0\mathbf{H}^0\cdot\mathbf{M}\,\mathrm{d}\mathbf{x} - \int_{\partial\Omega_2\cup\partial\Omega_3}\mathbf{t}^0\cdot\mathbf{u}\,\mathrm{d}S + \frac{\mu_0}{2}\int_{\mathbb{R}^3}|\nabla\phi|^2\,\mathrm{d}\mathbf{x} \tag{2.6}$$

subject to two constraints

$$\begin{array}{lll} \nabla\cdot\big(\mathbf{H}^{\mathrm{d}}+\mathbf{M}\chi_\Omega\big)=0 & \mathbf{H}^d=-\nabla\phi & \text{in } \mathbb{R}^3,\\ \nabla\cdot\boldsymbol{\sigma}=0 & \boldsymbol{\sigma}=\mathbf{C}[\boldsymbol{\varepsilon}-\boldsymbol{\varepsilon}^0(\mathbf{m})] & \text{in } \Omega, \end{array} \tag{2.7}$$

where ϕ is the magnetic potential resulting from $\nabla\times\mathbf{H}^{\mathrm{d}}=\mathbf{0}$, $\mathbf{H}^{\mathrm{d}}:\mathbb{R}^3\to\mathbb{R}^3$ the demagnetization or stray vector field, and the right-hand side of $(2.7)_2$ is the linear constitutive assumption with $\mathbf{C}$ as the elastic modulus. We assume that $\mathbf{C}$ is the positive-definite symmetric fourth-order tensor such that for $i,j,k,l=1,2,3$,

$$C_{ijkl}=C_{ijlk}=C_{klij}, \tag{2.8}$$

where C_{ijkl} are components of $\mathbf{C}$ in an orthonormal basis. Above in (2.6) $\mathbf{A}\in\mathbb{M}^{3\times3}_{\mathrm{s}}$ is a positive-definite tensor, $\mu_0=4\pi\times10^{-7}$ N/A^2 the coefficient of permeability of free space, and $W_{\mathrm{a}}:S^2\to\mathbb{R}$ the anisotropy energy density whose expression in terms of lowest-order terms for cubic and uniaxial crystals is

$$W_{\mathrm{a}}(\mathbf{m})=\begin{cases} K_0^{\mathrm{c}}+K_1^{\mathrm{c}}(m_1^{\mathrm{c}^2}m_2^{\mathrm{c}^2}+m_2^{\mathrm{c}^2}m_3^{\mathrm{c}^2}+m_3^{\mathrm{c}^2}m_1^{\mathrm{c}^2}) \\ \quad \text{cubic crystals,} \\ K_0^{\mathrm{u}}+K_1^{\mathrm{u}}\Big\{1-(\mathbf{m}\cdot\mathbf{e})^2\Big\} \\ \quad \text{uniaxial crystals,} \end{cases} \tag{2.9}$$

where K_0^{c}, K_0^{u} are irrelevant constants such that $W_{\mathrm{a}}(\mathbf{m})\geqslant 0$ for all $\mathbf{m}\in S^2$, K_1^{c}, K_1^{u} are *anisotropy constants* depending on materials and $\mathbf{e}$ is certain unit vectors.

Let us clarify the notation. Given $\mathbf{M}:\Omega\to M_{\mathrm{s}}S^2$, we solve (2.7) to obtain ϕ and $\boldsymbol{\varepsilon}$ and plug them back to (2.6) to obtain $\mathscr{E}(\mathbf{m})$. Maxwell's equation $(2.7)_1$ is of course solved over all space $\mathbb{R}^3$ with $\mathbf{M}=0$ outside Ω; we emphasize this by writing $\mathbf{M}\chi_\Omega$ where χ_Ω is the characteristic function of Ω explained above. Thus, by $(2.7)_1$, we mean:

$$\nabla\cdot(-\nabla\phi+\mathbf{M})=0 \quad \text{in } \Omega,$$

$$\nabla^2\phi=0 \quad \text{in } \mathbb{R}^3\setminus\overline{\Omega},$$

$$[\![-\nabla\phi+\mathbf{M}]\!]\cdot\mathbf{n}=0 \quad \text{on } \partial\Omega,$$

$$\phi\to0 \quad \text{as } |\mathbf{x}|\to\infty,$$

where $[\![\ ]\!]$ denotes the jump across the interface. Next, elastic equilibrium equation together with constitutive assumption in $(2.7)_2$ can be solved were the virtual distribution of body forces generated by $\mathbf{f}=-\nabla\cdot\mathbf{C}\boldsymbol{\varepsilon}^0(\mathbf{m})$ applied to the body as well as the constitutive relation changed as $\bar{\boldsymbol{\sigma}}=\mathbf{C}\boldsymbol{\varepsilon}$. In other words, we mean

$$\nabla\cdot\bar{\boldsymbol{\sigma}}+\mathbf{f}=\mathbf{0}, \quad \bar{\boldsymbol{\sigma}}=\mathbf{C}\boldsymbol{\varepsilon}, \quad \mathbf{f}=-\nabla\cdot\mathbf{C}\boldsymbol{\varepsilon}^0(\mathbf{m}). \tag{2.10}$$

Note that (2.10) is similar to the formulation of thermoelastostatics.

Each of the terms in the functional (2.6) has a physical interpretation. The first term, called the *exchange energy*, penalizes changes in the magnetization, and thus is interpreted as the energy of forming a magnetic domain wall. The second and third terms, the (total) *anisotropy energy*, is the energetic cost that the crystal must pay if the magnetization and strain deviate from the preferred states at that temperature; thus this builds in the information that the crystal prefers certain spontaneous magnetization and strain at a given temperature. Note that the zeros of W_{a} define the *easy axes*, i.e., the directions along which the crystal is magnetized most easily. For example, for cubic crystals, the case $K_1^{\mathrm{c}}>0$ in $(2.9)_1$ indicates the easy axes are along $\langle1\,0\,0\rangle_{\mathrm{c}}$ while $K_1^{\mathrm{c}}<0$ in $(2.9)_1$ indicates the easy axes are along the body diagonals, $\langle1\,1\,1\rangle_{\mathrm{c}}$. Similarly a positive K_1^{u} in $(2.9)_2$ describes an easy axis along the $\mathbf{e}$ direction while a negative K_1^{u} shows an easy plane perpendicular to the hard axis $\mathbf{e}$ for uniaxial crystals. The fourth, called the *Zeeman energy*, is the potential energy of the applied magnetic field, and this enforces the desire of the magnetization to align with the applied magnetic field. The fifth is of course the potential energy of the mechanical loading device.

The final term, called the *demagnetization energy* or *stray field energy*, is the magnetostatic self-energy associated with the magnetic field generated by the ferromagnetic crystal itself.

Finally, we consider a common case where the exchange tensor is isotropic; i.e., $\mathbf{A} = A\mathbf{I}$ where A is called the *exchange constant*. In addition, we assume the constrained displacement boundary condition if it exists; i.e., $\mathbf{u}^0 = \mathbf{0}\ \forall \mathbf{x} \in \partial\Omega_1 \cup \partial\Omega_3$. In this case, let $\boldsymbol{\sigma}^*$ be the auxiliary stress state satisfying

$$\begin{aligned} &\nabla \cdot \boldsymbol{\sigma}^* = 0, \quad \mathbf{x} \in \Omega, \\ &\boldsymbol{\sigma}^* \mathbf{n} = \mathbf{t}^0, \quad \mathbf{x} \in \partial\Omega_2, \\ &(\boldsymbol{\sigma}^* \mathbf{n}) \cdot \mathbf{l}_j = t_j^0, \quad \mathbf{x} \in \partial\Omega_3, \end{aligned} \tag{2.11}$$

where $\mathbf{l}_j$ is the same as that defined in (2.5). Thus, the total free energy of the ferromagnetic crystal (2.6) can be replaced by

$$\begin{aligned} \mathscr{E}(\mathbf{m}) = \int_\Omega \Big\{ & A|\nabla \mathbf{m}|^2 + W_{\mathrm{a}}(\mathbf{m}) \\ & + \frac{1}{2}\big[\boldsymbol{\varepsilon} - \boldsymbol{\varepsilon}^0(\mathbf{m})\big] \cdot \mathbf{C}\big[\boldsymbol{\varepsilon} - \boldsymbol{\varepsilon}^0(\mathbf{m})\big] \Big\} \mathrm{d}\mathbf{x} \\ & - \int_\Omega (\mu_0 \mathbf{H}^0 \cdot \mathbf{M} + \boldsymbol{\sigma}^* \cdot \boldsymbol{\varepsilon})\, \mathrm{d}\mathbf{x} \\ & + \frac{\mu_0}{2} \int_{\mathbb{R}^3} |\nabla \phi|^2 \, \mathrm{d}\mathbf{x} \end{aligned} \tag{2.12}$$

subject to the constraints (2.7). Suppose $\boldsymbol{\sigma}^* = \sigma_0 \boldsymbol{\xi} \otimes \boldsymbol{\xi}$ where $\sigma_0 > 0$ and $\boldsymbol{\xi}$ is the loading direction. It follows that magnetization is preferred to be aligned to maximize $\boldsymbol{\xi} \cdot \boldsymbol{\varepsilon}\boldsymbol{\xi}$ which is the projection of strain on the loading direction $\boldsymbol{\xi} \otimes \boldsymbol{\xi}$.

Eq. (2.12) with the help of the auxiliary stress $\boldsymbol{\sigma}^*$ is the micromagnetic formulation accounting for the effect of magnetoelastic interaction. It has been used by James and Wuttig (1998) and DeSimone and James (2002) to study various types of magnetic domains and will be adopted in the rest of this paper. Note that we have used the total strain $\boldsymbol{\varepsilon}$ in the fifth term of (2.12) instead of choosing magnetostrain $\boldsymbol{\varepsilon}^0(\mathbf{m})$ proposed by Hubert and Schäfer (1998) (see Eq. (3.61) in p. 148 there). The idea of using the total strain comes from the original formulation (2.6) which results from the principle of minimum potential energy in fundamental mechanics (Dym and Shames, 1973). The distinction between these two formulations is not significant for magnetic materials with extremely small magnetostriction (see Section 3.2 for explanation). However, it may lead to inconsistent results in certain materials with large magnetostriction (see Section 5.2).

2.3. Effective magnetic fields

The task in micromagnetics is to determine the magnetization $\mathbf{m}(\mathbf{x})$ which minimizes the free energy (2.12) subject to the constraints (2.7). A number of techniques to solve this minimization problem for rigid ferromagnetics have been proposed in the past decades which all are based on the variational method proposed by Brown (1962). Due to the constraint equation given by (2.2), Brown has considered a small variation of the direction of the magnetization vector instead of a small variation of the magnetization by an arbitrary function. The variational principle leads to modified Brown's equations accounting for the magnetoelastic effect

$$\begin{aligned} &\mathbf{m}(\mathbf{x}) \times \mathbf{H}^{\mathrm{eff}}(\mathbf{x}) = \mathbf{0} \quad \forall \mathbf{x} \in \Omega, \\ &\frac{\partial \mathbf{m}}{\partial \mathbf{n}}(\mathbf{x}) = \mathbf{0} \quad \forall \mathbf{x} \in \partial\Omega, \\ &\mathbf{H}^{\mathrm{eff}} = -\frac{1}{\mu_0 M_{\mathrm{s}}} \frac{\delta \mathscr{E}}{\delta \mathbf{m}} \\ &\qquad = \mathbf{H}^{\mathrm{e}} + \mathbf{H}^{\mathrm{a}} + \mathbf{H}^0 + \mathbf{H}^{\mathrm{s}} + \mathbf{H}^{\mathrm{d}}, \end{aligned} \tag{2.13}$$

where $\mathbf{H}^{\mathrm{eff}}$ is the *effective magnetic field* defined by the variational derivative of the free energy $-\frac{1}{\mu_0 M_{\mathrm{s}}} \frac{\delta \mathscr{E}}{\delta \mathbf{m}}$, $\mathbf{H}^{\mathrm{e}}$ the exchange magnetic field, $\mathbf{H}^{\mathrm{a}}$ the anisotropic magnetic field, $\mathbf{H}^0$ the external magnetic field, $\mathbf{H}^{\mathrm{s}}$ the stress-induced magnetic field and $\mathbf{H}^{\mathrm{d}}$ the demagnetization or stray field. The field $\mathbf{H}^0$ has been discussed in Section 2.2, $\mathbf{H}^{\mathrm{d}}$ is obtained by solving Maxwell's equation $(2.7)_1$, and the rest of magnetic fields are defined by

$$\begin{aligned} &\mathbf{H}^{\mathrm{e}} = \frac{2A}{\mu_0 M_{\mathrm{s}}} \nabla^2 \mathbf{m}, \\ &\mathbf{H}^{\mathrm{a}} = \frac{-1}{\mu_0 M_{\mathrm{s}}} \frac{\partial W_{\mathrm{a}}(\mathbf{m})}{\partial \mathbf{m}}, \\ &\mathbf{H}^{\mathrm{s}} = \frac{1}{\mu_0 M_{\mathrm{s}}} \mathbf{C}\big[\boldsymbol{\varepsilon} - \boldsymbol{\varepsilon}^0(\mathbf{m})\big] \cdot \frac{\partial \boldsymbol{\varepsilon}^0(\mathbf{m})}{\partial \mathbf{m}}, \end{aligned} \tag{2.14}$$

where $\boldsymbol{\varepsilon}$ is implicitly dependent on magnetization and is obtained by solving $(2.7)_2$. Note that (2.13) can be derived using the variational method similar to that for rigid ferromagnetics (Aharoni, 1996) while the stress-induced magnetic field $\mathbf{H}^{\mathrm{s}}$ is obtained by considering

$$\begin{aligned}
&\int_{\Omega}\delta\left\{\frac{1}{2}\mathbf{C}[\boldsymbol{\varepsilon}[\mathbf{u}]-\boldsymbol{\varepsilon}^{0}(\mathbf{m})]\cdot[\boldsymbol{\varepsilon}[\mathbf{u}]-\boldsymbol{\varepsilon}^{0}(\mathbf{m})]-\boldsymbol{\sigma}^{*}\cdot\boldsymbol{\varepsilon}[\mathbf{u}]\right\}\mathrm{d}\mathbf{x}\\
&\quad=\int_{\Omega}\left\{\mathbf{C}[\boldsymbol{\varepsilon}[\mathbf{u}]-\boldsymbol{\varepsilon}^{0}(\mathbf{m})]\cdot[\delta\boldsymbol{\varepsilon}[\mathbf{u}]-\delta\boldsymbol{\varepsilon}^{0}(\mathbf{m})]\right.\\
&\qquad\left.-\boldsymbol{\sigma}^{*}\cdot\delta\boldsymbol{\varepsilon}[\mathbf{u}]\right\}\mathrm{d}\mathbf{x}\\
&\quad=\int_{\Omega}\left\{(\boldsymbol{\sigma}-\boldsymbol{\sigma}^{*})\cdot\delta\boldsymbol{\varepsilon}[\mathbf{u}]-\boldsymbol{\sigma}\cdot\delta\boldsymbol{\varepsilon}^{0}(\mathbf{m})\right\}\mathrm{d}\mathbf{x}\\
&\quad=-\int_{\Omega}\boldsymbol{\sigma}\cdot\frac{\partial\boldsymbol{\varepsilon}^{0}(\mathbf{m})}{\partial\mathbf{m}}\delta\mathbf{m}\,\mathrm{d}\mathbf{x}+\int_{\partial\Omega}(\boldsymbol{\sigma}-\boldsymbol{\sigma}^{*})\mathbf{n}\cdot\delta\mathbf{u}\,\mathrm{d}s\\
&\quad=-\int_{\Omega}\boldsymbol{\sigma}\cdot\frac{\partial\boldsymbol{\varepsilon}^{0}(\mathbf{m})}{\partial\mathbf{m}}\delta\mathbf{m}\,\mathrm{d}\mathbf{x}
\end{aligned}$$

because of $\nabla\cdot\boldsymbol{\sigma}=\mathbf{0}$, $\nabla\cdot\boldsymbol{\sigma}^{*}=\mathbf{0}$, boundary conditions (2.5) and (2.11) and the fact that $\mathbf{C}$ is symmetric.

The effective magnetic field $\mathbf{H}^{\mathrm{eff}}$ provides an interpretation of the micromagnetic equations. From $(2.13)_1$ either the magnetization vector $\mathbf{m}$ is aligned along the effective magnetic field $\mathbf{H}^{\mathrm{eff}}$ at each point in the body Ω or the effective magnetic field $\mathbf{H}^{\mathrm{eff}}$ vanishes by itself since $\mathbf{m}\neq\mathbf{0}$ from (2.2). [1] In both cases the torque exerted on any magnetization vector has to be zero in static equilibrium. Finally, we are aware that (2.13) is the necessary condition for the minimization of total free energy. Magnetic domains satisfying the micromagnetic equations given by (2.13) are the local equilibrium magnetization.

[1] For example, if the crystal is large enough to reach the large-body limit (DeSimone, 1993), the exchange energy can be neglected and in this case the closure four domains results in $\mathbf{H}^{\mathrm{eff}}=\mathbf{0}$ in rigid magnetic cubic crystals (Hubert and Schäfer, 1998).

2.4. Magnetization dynamics

If Brown's equations (2.13) do not hold at some points, the nonzero torque $\mathbf{m}\times\mathbf{H}^{\mathrm{eff}}$ provides a precession of the magnetization around the effective field. Indeed, the dynamic description of micromagnetic processes in a ferromagnetic material can be described by the famous LLG evolution equation (Landau and Lifshitz, 1935; Gilbert, 1955)

$$\frac{\mathrm{d}\mathbf{m}}{\mathrm{d}t}=-\gamma\mathbf{m}\times\mathbf{H}^{\mathrm{eff}}-\alpha\gamma\mathbf{m}\times(\mathbf{m}\times\mathbf{H}^{\mathrm{eff}}),\tag{2.15}$$

where t is the time. Above the first term on the right-hand side is the gyromagnetic term, with $\gamma\approx 2.21\times10^{5}$ m/A/s being the gyromagnetic ratio. The second on the right-hand side is the damping term, with α being the dimensionless damping coefficient. The damping term allows the magnetization to turn towards the effective field until both vectors are parallel in the static solution. It is obvious that Brown's micromagnetic equations can be viewed as a particular case of (2.15), giving the static equilibrium when there is no change in time. The boundary conditions here are the same as that in the static equilibrium given by (2.13).

Clearly from (2.15) the torque $\mathbf{m}\times\mathbf{H}^{\mathrm{eff}}$ provides the driving force for the evolution of magnetization, and the small quantity of $|\frac{\mathrm{d}\mathbf{m}}{\mathrm{d}t}|$ implies the (local) equilibrium magnetization configuration. In fact, the evolution of magnetization described by LLG equation (2.15) also implies the decrease of the total free energy (2.12), and this can be understood by considering

$$\begin{aligned}
\frac{1}{\mu_{0}M_{\mathrm{s}}}\frac{\mathrm{d}\mathscr{E}}{\mathrm{d}t}&=\int_{\Omega}(-\mathbf{H}^{\mathrm{eff}}\cdot\dot{\mathbf{m}})\,\mathrm{d}\mathbf{x}\\
&=-\int_{\Omega}\mathbf{H}^{\mathrm{eff}}\cdot\big(-\gamma\mathbf{m}\times\mathbf{H}^{\mathrm{eff}}\\
&\qquad-\alpha\gamma\mathbf{m}\times(\mathbf{m}\times\mathbf{H}^{\mathrm{eff}})\big)\mathrm{d}\mathbf{x}\\
&=\alpha\gamma\int_{\Omega}\mathbf{H}^{\mathrm{eff}}\cdot\left\{(\mathbf{m}\cdot\mathbf{H}^{\mathrm{eff}})\mathbf{m}-\mathbf{H}^{\mathrm{eff}}\right\}\mathrm{d}\mathbf{x}\\
&=\alpha\gamma\int_{\Omega}\left\{\left|\mathbf{m}\cdot\mathbf{H}^{\mathrm{eff}}\right|^{2}-\left|\mathbf{H}^{\mathrm{eff}}\right|^{2}\right\}\mathrm{d}\mathbf{x}\leqslant 0
\end{aligned}\tag{2.16}$$

due to the famous Cauchy–Schwartz inequality and $|\mathbf{m}|=1$. The more general form of dissipation

mechanism other than LLG equation in rigid micromagnetics can be found in the recent work of Podio-Guidugli (2001).

As the result of (2.16), LLG equation cannot only provide the information of time evolution of magnetization, but also offers a convenient tool to study the static equilibrium magnetization. As a matter of fact, the integration algorithm of LLG and LLG-like equations of motions have been used widely in literature to study domain walls and equilibrium magnetization distributions by assuming $\left|\frac{d\mathbf{m}}{dt}\right|$ is less than the prescribed small value (see Nakatani et al. (1989) and Berkov et al. (1993) for a detailed description). Thus from now on we will use (2.15) as our fundamental tool to investigate magnetic domain patterns and their evolution for various magnetostrictive crystals. Other methods to solve (2.13) directly can be found in Aharoni and Jakubovics (1986), LaBonte (1969) and Miltat et al. (1989).

3. Solutions of constrained equations

In magnetostatics the solution of the magnetic potential ϕ in $(2.7)_1$ can be derived using the Green function method introduced by the potential theory (Kellogg, 1969). There are no problems with boundary conditions or material properties as the Green function is independent of both of them. Unfortunately the analogous procedure meets certain difficulties for magnetoelastic interactions. Essentially we try to solve

$$\nabla \cdot (\mathbf{C}\boldsymbol{\varepsilon}[\mathbf{u}]) = \nabla \cdot (\mathbf{C}\boldsymbol{\varepsilon}^0(\mathbf{m})) \quad \forall \mathbf{x} \in \Omega \tag{3.1}$$

which seems to be similar to

$$\nabla \cdot (\nabla \phi) = \nabla \cdot (\mathbf{M}\chi_\Omega) \quad \forall \mathbf{x} \in \mathbb{R}^3 \tag{3.2}$$

once the magnetization $\mathbf{M}(\mathbf{x})$ is given at each point in Ω. However, (3.1) is in general much more difficult to be solved than (3.2) because of the complications associated with the elastic tensor $\mathbf{C}$ and boundary conditions. It is in principle not possible to extract the fourth-order tensor $\mathbf{C}$ out of the differential equation in (3.1). In addition, this tensor is material dependent, so is the solution of (3.1). Finally, the Green function for (3.1) is dependent on the domain Ω itself and the associated boundary conditions given by (2.5) while the Green function for the magnetic equation (3.2) is independent of domains and materials. As a result, there are no generally applicable procedures for the solution of the elastic case (3.1), at least, explicit expressions similar to the magnetic solution. We are then forced to resolve such a difficulty either by a crude approximation (see Section 3.2) or by certain sophisticated numerical schemes (see Section 3.3).

3.1. Maxwell equation

The solution of the magnetic potential ϕ in $(2.7)_1$ can be easily obtained by Green function method. We refer to Jackson (1962) and Kellogg (1969) for the detailed derivation and only list the formulation. Suppose the ferromagnetic crystal is a finite body occupying a domain Ω in the three-dimensional space, the magnetic potential is given by

$$\phi(\mathbf{x}) = \frac{1}{4\pi}\left\{ \int_\Omega \frac{-\nabla_{\mathbf{x}'} \cdot \mathbf{M}(\mathbf{x}')}{|\mathbf{x}-\mathbf{x}'|}\, d\mathbf{x}' + \int_{\partial\Omega} \frac{\mathbf{M}(\mathbf{x}') \cdot \mathbf{n}}{|\mathbf{x}-\mathbf{x}'|}\, dS_{\mathbf{x}'} \right\}, \tag{3.3}$$

while for an infinitely long ferromagnetic cylinder along the $\mathbf{e}_3$ direction, the magnetic potential is given by

$$\phi(\mathbf{x}_p) = \frac{1}{2\pi}\left\{ \int_\Omega \left(\nabla_{\mathbf{x}'_p} \cdot \mathbf{M}(\mathbf{x}'_p)\right) \ln|\mathbf{x}_p - \mathbf{x}'_p|\, d\mathbf{x}'_p - \int_{\partial\Omega} \left(\mathbf{M}(\mathbf{x}'_p) \cdot \mathbf{n}\right) \ln|\mathbf{x}_p - \mathbf{x}'_p|\, dS_{\mathbf{x}'_p} \right\}, \tag{3.4}$$

where $\mathbf{x}_p = (x_1, x_2)$ and Ω here is the finite in-plane cross section of the long cylinder. Note that the Green functions for (3.3) and (3.4) are the Newtonial potential $\frac{-1}{4\pi}\frac{1}{|\mathbf{x}|}$ and logarithmic potential $\frac{1}{2\pi}\ln|\mathbf{x}_p|$. Both functions are independent of solid boundaries and material properties.

3.2. Equilibrium equation by approximation

There are in general no explicit expressions similar to (3.3) or (3.4) for the solution of elastic

equilibrium equation $(2.7)_2$. To overcome such a difficulty and complexity, a very common approach in literature is to replace the total strain $\boldsymbol{\varepsilon}$ by magnetostrain tensor $\boldsymbol{\varepsilon}^0(\mathbf{m})$ (Cullity, 1972; Cullen et al., 1997; Callegaro and Puppin, 1997); i.e.,

$$\boldsymbol{\varepsilon} \approx \boldsymbol{\varepsilon}^0 \tag{3.5}$$

in (2.12). As a result, (2.12) becomes

$$\mathscr{E}_{\text{approx}}(\mathbf{m}) = \int_\Omega \left\{ A|\nabla \mathbf{m}|^2 + \widetilde{W}_{\text{a}}(\mathbf{m}) - \mu_0 \mathbf{H}^0 \cdot \mathbf{M} \right\} \mathrm{d}\mathbf{x} + \frac{\mu_0}{2} \int_{\mathbb{R}^3} |\nabla \phi|^2 \, \mathrm{d}\mathbf{x}, \tag{3.6}$$

where $\widetilde{W}_{\text{a}}(\mathbf{m})$ is the modified anisotropic energy density defined by

$$\widetilde{W}_{\text{a}}(\mathbf{m}) = W_{\text{a}}(\mathbf{m}) - \boldsymbol{\sigma}^* \cdot \boldsymbol{\varepsilon}^0(\mathbf{m}). \tag{3.7}$$

Eq. (3.6) is the same as that for rigid ferromagnetics except that the anisotropy energy density $W_{\text{a}}(\mathbf{m})$ is replaced by $\widetilde{W}_{\text{a}}(\mathbf{m})$. Note that (3.7) shows that the energy of applied loads becomes another source of magnetic anisotropy energy while the magnetostrictive self-energy vanishes; i.e., the external stress causes the induction of a magnetostrictive uniaxial anisotropy, usually called stress-induced anisotropy (Ross et al., 1996; Deng et al., 1997). The material is then treated as a rigid ferromagnetics with varying magnetic easy axes depending on external stress. This approximation, which we call relaxed approach, neglects the intrinsic stress due to the assumption of (3.5). Question arises for such an approximation because of loss of strain compatibility. Kinematic compatibility requires (Gurtin, 1972)

$$\nabla \times \nabla \times \boldsymbol{\varepsilon} = \mathbf{0} \tag{3.8}$$

while (3.8) may not be satisfied if $\boldsymbol{\varepsilon}(\mathbf{x})$ is simply replaced by $\boldsymbol{\varepsilon}^0(\mathbf{m}(\mathbf{x}))$ for arbitrary magnetization at each point $\mathbf{x}$.

The stress-induced magnetic field defined by (2.14) becomes

$$\mathbf{H}_{\text{s}}^{\text{r}} = \frac{1}{\mu_0 M_{\text{s}}} \boldsymbol{\sigma}^* \cdot \frac{\partial \boldsymbol{\varepsilon}^0(\mathbf{m})}{\partial \mathbf{m}}, \tag{3.9}$$

where (3.9) is derived by the variational derivative of the relaxed energy given by (3.6) and the superscript r in $\mathbf{H}_{\text{s}}^{\text{r}}$ emphasizes that this field is obtained by the relaxed approach. So clearly from (3.9) $\mathbf{H}_{\text{s}}^{\text{r}}$ is zero if the external stress $\boldsymbol{\sigma}^*$ is absent; and therefore, the ferromagnetic crystal is treated as a rigid material regardless of the possible existence of intrinsic stress. Hence, this relaxed approach is expected to be a crude approximation for magnetic materials with large magnetostriction at zero applied loads.

Finally, we remark on the current development of active materials such as shape-memory alloys, ferroelectrics and ferromagnetics. In the modern theory of these materials, the study of microstructure requires the total strain $\boldsymbol{\varepsilon}(\mathbf{x})$ to be replaced by the stress-free strain $\boldsymbol{\varepsilon}^0(\mathbf{x})$ at each point if $\boldsymbol{\varepsilon}^0$ belongs to a class of strains $\mathscr{S}$ in which strains are symmetry related and compatible with one another. The magnitudes of these strains do not need to be small, and in some materials such as shape-memory materials, they are very large. The intrinsic stress vanishes since strains in $\mathscr{S}$ are compatible. As a result, the effect of external stress on microstructure redistribution can indeed be approximated by considering the following potential energy:

$$-\boldsymbol{\sigma}^* \cdot \langle \boldsymbol{\varepsilon}^0 \rangle,$$

where $\langle \cdot \rangle$ denotes the average over the body. The favorable microstructure is expected to the one which minimizes the above potential energy. While the results predicted by this theory have been found to be very useful in many applications, one drawback of this approach is that the energy barrier caused by intrinsic stress as microstructure evolves may prevent favorable states from being achieved, and the estimate of this barrier is in general not revealed by this approach. The systematic description of this theory for various active materials can be found in Bhattacharya (1993), Shu and Bhattacharya (2001), Li and Bhattacharya (in preparation) and DeSimone and James (2002).

3.3. Equilibrium equation by modified boundary element method

As described in the introduction of Section 3, it is not an easy task to solve the elastic equilibrium equation given by $(2.7)_2$ for arbitrary magnetostrain $\boldsymbol{\varepsilon}^0(\mathbf{m})$. We thus restrict ourselves to consider

two common cases: one is for a thin film and the other for a long cylinder with arbitrary finite cross section. For both cases, we may assume

$$\mathbf{m} = \mathbf{m}(x_1, x_2) \in S^2, \quad \mathbf{u} = \mathbf{u}(x_1, x_2) \in \mathbb{R}^3. \tag{3.10}$$

The problem is now simplified to be two-dimensional in space, but the magnetization $\mathbf{m}$ is still free to rotate in three dimensions. The simplification from (3.10) does not lead to the direct solution of $(2.7)_2$ in closed forms. Instead, it provides an opportunity to solve the elastic equilibrium equation by certain sophisticated numerical schemes. There are two major numerical methods: finite element method (FEM) and boundary element method (BEM). Both methods have their own merits and are applied to a variety of scientific problems according to their specific needs. Traditionally both methods have better numerical precision in displacement $\mathbf{u}$ than strain $\boldsymbol{\varepsilon}$ (Oden and Reddy, 1976). However, in our present case, the main variable we need is strain $\boldsymbol{\varepsilon}$ rather than displacement $\mathbf{u}$ (see $(2.14)_3$). We thus need to look for a new strain-based formalism. Indeed, Wu et al. (1992) and Wu (2000) have proposed a new boundary integral equation formalism for two-dimensional anisotropic elasticity without considering the effect of body force (i.e., $\mathbf{f} = \mathbf{0}$ in (2.10)). This formulation is presented in complex-variable using Stroh formalism for anisotropic elasticity (Stroh, 1958). The advantage of it is that in numerical implementation the boundary integrals can be integrated analytically along each element. In addition, it can be shown that this formalism has better numerical precision in variable strain as well as faster rate of convergence than conventional displacement-based schemes. We thus propose to solve $(2.7)_2$ by extending their approach to the case accounting for the effect of virtual body force resulting from the divergence of magneto-stress (i.e., $\mathbf{f} \neq \mathbf{0}$ in (2.10)).

Let an elastic body occupy a long cylindrical domain with finite in-plane cross section denoted by Ω as shown in Fig. 2. Note that we have slightly abused the notation Ω which was used to denote the domain occupied by the whole ferromagnetic body. Suppose there are no body force densities and stress is related to strain by $\boldsymbol{\sigma} = \mathbf{C}\boldsymbol{\varepsilon}$ where $\mathbf{C}$ is the elastic modulus satisfying (2.8). Let $\mathbf{a}_k$ and p_k

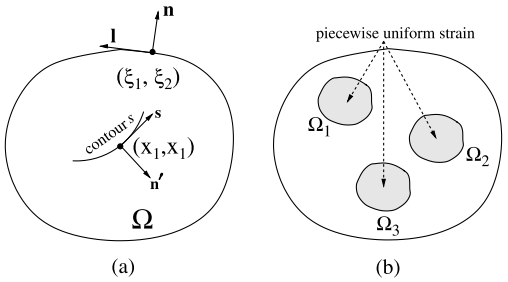

Fig. 2. (a) An elastic body occupies a long cylindrical domain with in-plane cross section denoted by Ω. (b) The strain $\boldsymbol{\varepsilon}^0$ is assumed to be piecewise uniform in subdomains $\Omega_i \subset \Omega$, $i = 1, \ldots, B$. Only three subdomains are shown here.

be the eigenvectors and eigenvalues of the following equation:

$$\left[\mathbf{Q} + (\mathbf{R} + \mathbf{R}^{\mathrm{T}})p_k + \mathbf{T}p_k^2\right]\mathbf{a}_k = \mathbf{0} \quad (\text{no sum over } k), \tag{3.11}$$

where

$$Q_{ik} = C_{i1k1}, \quad R_{ik} = C_{i1k2}, \quad T_{ik} = C_{i2k2}, \quad i,k = 1, \ldots, 3,$$

and C_{ijkl} are the components of the elasticity tensor $\mathbf{C}$ in some reference basis. As p_k can be shown to be nonreal (Stroh, 1958; Ting, 1996), we thus take p_k, $k = 1, 2, 3$, with positive imaginary part for definiteness. Let $\mathbf{A} = (\mathbf{a}_1|\mathbf{a}_2|\mathbf{a}_3)$ be the 3×3 matrix whose ith column is replaced by the column vector $\mathbf{a}_i$ defined by (3.11). Further, we define the matrix $\mathbf{B}$ related with $\mathbf{A}$ by

$$\mathbf{B} = \mathbf{R}^{\mathrm{T}}\mathbf{A} + \mathbf{T}\mathbf{A}\mathbf{P}, \tag{3.12}$$

where $\mathbf{P} = \mathrm{diag}[p_1, p_2, p_3]$; i.e., a matrix with diagonal entries replace by p_1, p_2, p_3 and zero in the rest of entries.

Set

$$z = x_1 + \mathrm{i}x_2, \quad \zeta = \xi_1 + \mathrm{i}\xi_2, \tag{3.13}$$

where z and ζ are field and source points in the complex plane and $\mathrm{i} = \sqrt{-1}$ is the imaginary number. Now let $(x_1, x_2) \in \overline{\Omega}$, $(\xi_1, \xi_2) \in \partial\Omega$ and $\mathbf{l}, \mathbf{n}$ are unit tangent and outward normal vectors to the boundary $\partial\Omega$ as shown in Fig. 2(a). Let $\frac{\partial \mathbf{u}}{\partial s}(z)$ and $\mathbf{t}(z)$ be the displacement gradient and traction at point z along an arbitrary contour s. Both can be related by the tangential displacement gradient

$\mathbf{d_l} = \frac{\partial \mathbf{u}}{\partial \mathbf{l}}$ and traction $\mathbf{t_n}$ on the boundary $\partial\Omega$ by the following dual set of boundary integral equations proposed by Wu et al. (1992):

$$\beta \frac{\partial \mathbf{u}}{\partial s}(z) = \int_{\partial\Omega} \left\{ \frac{\partial \mathbf{U}}{\partial s}(z,\zeta)\mathbf{t_n}(\zeta) - \frac{\partial \mathbf{W}}{\partial s}(z,\zeta)\mathbf{d_l}(\zeta) \right\} \mathrm{d}l, \tag{3.14}$$

$$\beta \mathbf{t}(z) = \int_{\partial\Omega} \left\{ -\frac{\partial \mathbf{W}^{\mathrm{T}}}{\partial s}(z,\zeta)\mathbf{t_n}(\zeta) + \frac{\partial \mathbf{V}}{\partial s}(z,\zeta)\mathbf{d_l}(\zeta) \right\} \mathrm{d}l, \tag{3.15}$$

where $\mathrm{d}l = \sqrt{\mathrm{d}\xi_1^2 + \mathrm{d}\xi_2^2}$, $\beta = 1$ in Ω and $\beta = \frac{1}{2}$ at the smooth boundary $\partial\Omega$, and

$$\mathbf{U}(z,\zeta) = \Re[\mathbf{A}\mathbf{G}(z,\zeta)\mathbf{A}^{\mathrm{T}}],$$
$$\mathbf{W}(z,\zeta) = \Re[\mathbf{A}\mathbf{G}(z,\zeta)\mathbf{B}^{\mathrm{T}}],$$
$$\mathbf{V}(z,\zeta) = \Re[\mathbf{B}\mathbf{G}(z,\zeta)\mathbf{B}^{\mathrm{T}}].$$

Above $\Re$ stands for the real part, $\mathbf{A}$ and $\mathbf{B}$ are defined by (3.11) and (3.12), and the matrix function $\mathbf{G}(z,\zeta)$ is defined by

$$\mathbf{G}(z,\zeta) = \frac{1}{\mathrm{i}\pi} \begin{pmatrix} \ln(z_1-\zeta_1) & 0 & 0 \\ 0 & \ln(z_2-\zeta_2) & 0 \\ 0 & 0 & \ln(z_3-\zeta_3) \end{pmatrix}, \tag{3.16}$$

where

$$z_k = x_1 + p_k x_2, \quad \zeta_k = \xi_1 + p_k \xi_2. \tag{3.17}$$

Eqs. (3.14) and (3.15) with $\beta = \frac{1}{2}$ provide a pair of boundary integral equations for the tangential displacement gradient and traction if the contour s is chosen to coincide with the boundary. Either (3.14) or (3.15) can be solved to obtain the unknown tangential displacement gradient or traction. Once the unknown boundary data is determined, the displacement gradient and traction in any directions inside the domain Ω can therefore be computed from (3.14) and (3.15) with $\beta = 1$.

Now suppose that the constitutive relation becomes $\boldsymbol{\sigma}(\mathbf{x}) = \mathbf{C}[\boldsymbol{\varepsilon}(\mathbf{x}) - \boldsymbol{\varepsilon}^0(\mathbf{x})]$ where $\boldsymbol{\varepsilon}^0$ is the eigenstrain. Assume there is a set of disjoint domains $\Omega_i \subset \Omega$, $i = 1, \ldots, B$, such that $\boldsymbol{\varepsilon}^0(\mathbf{x}) = \mathbf{0}$ if $\mathbf{x} \in \Omega \setminus \overline{(\Omega_1 \cup \cdots \cup \Omega_B)}$ and is uniform in Ω_i as shown in Fig. 2(b). The eigenstrain $\boldsymbol{\varepsilon}^0$ may take different values for different subdomains Ω_i. As the traction is balanced (continuous) across the boundary $\partial\Omega_i$, we have

$$\lim_{\substack{\mathbf{x}\in\Omega_i \\ \mathbf{x}\to\partial\Omega_i}} \bar{\boldsymbol{\sigma}}\mathbf{n}_i - \lim_{\substack{\mathbf{x}\in\Omega\setminus\Omega_i \\ \mathbf{x}\to\partial\Omega_i}} \bar{\boldsymbol{\sigma}}\mathbf{n}_i = \boldsymbol{\sigma}^0\mathbf{n}_i, \tag{3.18}$$

where $\mathbf{n}_i$ is the unit outward normal to the boundary $\partial\Omega_i$, and

$$\bar{\boldsymbol{\sigma}} = \mathbf{C}\boldsymbol{\varepsilon}, \quad \boldsymbol{\sigma}^0 = \mathbf{C}\boldsymbol{\varepsilon}^0. \tag{3.19}$$

Physically, it means there is a prescribed body force density $\boldsymbol{\sigma}^0(\mathbf{x})\mathbf{n}_i(\mathbf{x})\chi_{\partial\Omega_i}$ supported on the boundary of each Ω_i if the constitutive law were replaced by $\bar{\boldsymbol{\sigma}} = \mathbf{C}\boldsymbol{\varepsilon}$ throughout the whole domain Ω. To account for such an effect, note that Wu et al. (1992) have pointed out that the displacement gradient (3.14) and traction (3.15) along an arbitrary contour s in a finite body Ω can be viewed as those due to the dislocation dipole $-\mathbf{u}\,\mathrm{d}l$ and body force density $\mathbf{t_n}$ supported on the boundary $\partial\Omega$ in an *infinite space*. As a consequence, the displacement gradient and traction along any arbitrary contour s due to piecewise uniform eigenstrain $\boldsymbol{\varepsilon}^0(\mathbf{x})$ can be obtained from (3.14), (3.15), (3.18), and (3.19) and are given by

$$\beta \frac{\partial \mathbf{u}}{\partial s}(z) = \int_{\partial\Omega} \left\{ \frac{\partial \mathbf{U}}{\partial s}(z,\zeta)\mathbf{t_n}(\zeta) - \frac{\partial \mathbf{W}}{\partial s}(z,\zeta)\mathbf{d_l}(\zeta) \right\} \mathrm{d}l + \sum_i \int_{\partial\Omega_i} \frac{\partial \mathbf{U}}{\partial s}(z,\zeta)\mathbf{t}^0_{\mathbf{n}_i}(\zeta)\,\mathrm{d}l, \tag{3.20}$$

$$\beta\left(\mathbf{t}(z) + \sum_i \mathbf{t}^0(z)\chi_{\Omega_i}\right) = \int_{\partial\Omega} \left\{ -\frac{\partial \mathbf{W}^{\mathrm{T}}}{\partial s}(z,\zeta)\mathbf{t_n}(\zeta) + \frac{\partial \mathbf{V}}{\partial s}(z,\zeta)\mathbf{d_l}(\zeta) \right\} \mathrm{d}l - \sum_i \int_{\partial\Omega_i} \frac{\partial \mathbf{W}^{\mathrm{T}}}{\partial s}(z,\zeta)\mathbf{t}^0_{\mathbf{n}_i}(\zeta)\,\mathrm{d}l, \tag{3.21}$$

where

$$\mathbf{t}^0(z) = (\mathbf{C}\boldsymbol{\varepsilon}^0(z))\mathbf{n}', \quad \mathbf{t}^0_{\mathbf{n}_i}(\zeta) = (\mathbf{C}\boldsymbol{\varepsilon}^0(\zeta))\mathbf{n}_i,$$

where $\mathbf{n}'$ and $\mathbf{n}_i$ are the unit normals to the contour s and the boundary $\partial\Omega_i$, respectively. The unknown tangential displacement gradient or traction can be obtained by solving (3.20) and (3.21) if the contour s is chosen to coincide with the boundary. Once the unknown boundary data is

determined, the displacement gradient and traction in any direction inside Ω can therefore be computed from (3.20) and (3.21) with $\beta = 1$.

In magnetostrictive material, the magnetostrain $\boldsymbol{\varepsilon}^0(\mathbf{m})(\mathbf{x})$ is in general not piecewise constant inside Ω. However, we may assume that it is uniform in each small cell in which the magnetization $\mathbf{m}$ is approximated to be constant. In this situation, we can use (3.20) and (3.21) to solve $(2.7)_2$ numerically and the details are provided in the next section.

Finally, the previous analysis is applied to a long cylinder with finite cross section. In the case of thin films, (3.20) and (3.21) are still valid with slight modification. Under the plane stress assumption, the elastic modulus $\mathbf{C}$ is replaced by the generalized plane stress modulus $\mathbf{C}^p$, and only the in-plane components of magnetostrain $\boldsymbol{\varepsilon}^0$ are taken into account in the formulation of both (3.20) and (3.21). To make it clear, let the film occupy the domain $\Omega = S \times (0,h)$ where h is the film thickness and S the in-plane cross section of the film. For simplicity, assume that S is a square domain; i.e., $S = (0,L)^2$. Further, decompose $\mathbf{u} = \mathbf{u}^p + \tilde{\mathbf{b}}x_3$ where $\mathbf{u}^p = (u_1^p(x_1,x_2), u_2^p(x_1,x_2), 0)$ and $\tilde{\mathbf{b}} = (2\tilde{b}_1(x_1,x_2), 2\tilde{b}_2(x_1,x_2), \tilde{b}_3(x_1,x_2))$. Set $b_1^* = \tilde{b}_1 - \varepsilon_{31}^0$, $b_2^* = \tilde{b}_2 - \varepsilon_{32}^0$ and $b_3^* = \tilde{b}_3 - \varepsilon_{33}^0$ and (b_1^*, b_2^*, b_3^*) is the minimizer of $\inf_{\mathbf{b}\in\mathbb{R}^3} \frac{1}{2}\mathbf{E}\cdot\mathbf{CE}$ where $\mathbf{b} = (b_1, b_2, b_3)$ and

$$\mathbf{E} = \begin{pmatrix} \varepsilon_{11}^p - \varepsilon_{11}^0 & \varepsilon_{12}^p - \varepsilon_{12}^0 & b_1 \\ \varepsilon_{21}^p - \varepsilon_{21}^0 & \varepsilon_{22}^p - \varepsilon_{22}^0 & b_2 \\ b_1 & b_2 & b_3 \end{pmatrix}. \tag{3.22}$$

Let $\bar{\mathbf{u}} = \frac{\mathbf{u}}{L}$ and $\bar{\mathbf{x}} = \frac{\mathbf{x}}{L}$. It follows from Shu (2002) that the total magnetostrictive energy per unit volume can be shown to be

$$\begin{aligned} &\frac{1}{hL^2}\int_\Omega \frac{1}{2}(\boldsymbol{\varepsilon} - \boldsymbol{\varepsilon}^0)\cdot\mathbf{C}(\boldsymbol{\varepsilon} - \boldsymbol{\varepsilon}^0)\,\mathrm{d}\mathbf{x} \\ &\quad = U_0 + \left(\frac{h}{L}\right)U_1 + \mathrm{o}\left(\frac{h}{L}\right), \end{aligned} \tag{3.23}$$

where $\frac{\mathrm{o}(\alpha)}{\alpha} \to 0$ as $\alpha \to 0$ and

$$\begin{aligned} U_0 &= \int_0^1\int_0^1 \frac{1}{2}\left(\boldsymbol{\varepsilon}^p - \boldsymbol{\varepsilon}^{0p}\right)\cdot\mathbf{C}^p\left(\boldsymbol{\varepsilon}^p - \boldsymbol{\varepsilon}^{0p}\right)\mathrm{d}\bar{x}_1\,\mathrm{d}\bar{x}_2, \\ U_1 &= \int_0^1\int_0^1 2\boldsymbol{\varepsilon}^b\cdot\mathbf{C}^p\left(\boldsymbol{\varepsilon}^p - \boldsymbol{\varepsilon}^{0p}\right)\mathrm{d}\bar{x}_1\,\mathrm{d}\bar{x}_2. \end{aligned} \tag{3.24}$$

Above, $\mathbf{C}^p$ is the generalized plane stress modulus, $\boldsymbol{\varepsilon}^{0p} \in \mathbb{M}_{\mathrm{s}}^{2\times 2}$ the in-plane magnetostrain tensor with components $\varepsilon_{\alpha\beta}^{0p} = \varepsilon_{\alpha\beta}^0$, $\boldsymbol{\varepsilon}^p \in \mathbb{M}_{\mathrm{s}}^{2\times 2}$ the in-plane strain tensor with components defined by

$$\varepsilon_{\alpha\beta}^p = \frac{1}{2}\left(\frac{\partial u_\alpha^p}{\partial x_\beta} + \frac{\partial u_\beta^p}{\partial x_\alpha}\right),$$

and $\boldsymbol{\varepsilon}^b \in \mathbb{M}_{\mathrm{s}}^{2\times 2}$ with components defined by

$$\varepsilon_{\alpha\beta}^b = \frac{1}{2}\left(\frac{\partial b_\alpha^*}{\partial x_\beta} + \frac{\partial b_\beta^*}{\partial x_\alpha}\right)$$

for $\alpha, \beta = 1, 2$. As a consequence from (3.23), we only need to consider the energy U_0 if the ratio $\frac{h}{L}$ is small, and minimizing it yields the reduced elastic equilibrium equation $\nabla_p \cdot \boldsymbol{\sigma}^p = \mathbf{0}$ where $\boldsymbol{\sigma}^p = \mathbf{C}^p[\boldsymbol{\varepsilon}^p - \boldsymbol{\varepsilon}^{0p}]$ and ∇_p is the in-plane gradient. Notice that U_1 can be completely determined once U_0 is known.

4. Numerical algorithm

4.1. Integration of LLG equation

The integration of LLG equation (2.15) is based on the algorithm provided by the National Institute of Standards and Technology (NIST) of the US (Donahue, 2000) which has been used extensively in a variety of applications and fundamental research (Donahue, 1998; Crew and Lewis, 2001; Thiaville et al., 2002). It is based on the finite difference method by replacing the continuous solution of magnetic domains by a discrete set of lattice. At each lattice point the differential operators are replaced by finite difference operators using a second-order predictor–corrector technique of the Adams type, and the conditions on the boundary of magnetic domains are replaced with their discrete counterparts.

The exchange energy is evaluated using the eight-neighbor bilinear interpolation (Donahue and McMichael, 1997), the anisotropy and Zeeman energy terms are computed assuming constant magnetization in each mesh. The stray field is calculated as the convolution of the magnetization against a kernel describing the mesh to mesh magnetostatic interaction. The convolution is computed using Fast Fourier Transform. The

stress-induced magnetic field is based on the modified BEM described in Section 3.3 and the algorithm is provided in Section 4.2.

The modeling system is a two-dimensional thin film with film thickness much smaller than its lateral dimensions. Thus the plane stress condition is used throughout the calculation. We also assume that the film thickness is on or smaller than the order of magnetic exchange length defined by $\pi\sqrt{\frac{A}{K_1}}$ where A, K_1 are exchange and anisotropy parameters (see (2.12) and (2.9). So we may postulate that the magnetization is the function of in-plane variables x_1, x_2 only. The film is divided into a large number of small square cells. Inside each cell the magnetic moment $\mathbf{m}$ is free to rotate in three dimensions but its magnitude is kept to be unity. The Neumann type of magnetic boundary condition given by (2.13) is assumed throughout the calculation.

4.2. Stress-induced magnetic field

We recall that the stress-induced magnetic field defined by (2.14) is

$$\mathbf{H}_{\mathrm{s}}^{\mathrm{c}} = \frac{1}{\mu_0 M_{\mathrm{s}}}\boldsymbol{\sigma}\cdot\frac{\partial\boldsymbol{\varepsilon}^0(\mathbf{m})}{\partial\mathbf{m}}, \tag{4.1}$$

where the superscript 'c' denotes that this field is obtained by the constrained approach in which the constrained (equilibrium) equation $(2.7)_2$ has to be solved for each magnetization configuration. Note that $\mathbf{H}_{\mathrm{s}}^{\mathrm{c}}$ is different from $\mathbf{H}_{\mathrm{s}}^{\mathrm{r}}$ defined by the relaxed approach (3.9). We have implemented two algorithms to compute $\mathbf{H}_{\mathrm{s}}^{\mathrm{c}}$ and $\mathbf{H}_{\mathrm{s}}^{\mathrm{r}}$ in order to compare the differences between these two methods. As $\mathbf{H}_{\mathrm{s}}^{\mathrm{r}}$ is quite easy to be implemented, we now focus on the numerical implementation of $\mathbf{H}_{\mathrm{s}}^{\mathrm{c}}$ next.

We first concentrate on the term $\frac{\partial\boldsymbol{\varepsilon}^0(\mathbf{m})}{\partial\mathbf{m}}$. Recall that $\{\mathbf{e}_1^{\mathrm{c}}, \mathbf{e}_2^{\mathrm{c}}, \mathbf{e}_3^{\mathrm{c}}\}$ is an orthonormal crystal basis and $\{\mathbf{e}_1, \mathbf{e}_2, \mathbf{e}_3\}$ the orthonormal basis in the reference configuration. They are related by

$$\mathbf{e}_i^{\mathrm{c}} = \mathbf{R}\mathbf{e}_i, \quad R_{ij} = \mathbf{e}_i\cdot\mathbf{R}\mathbf{e}_j = \mathbf{e}_i\cdot\mathbf{e}_j^{\mathrm{c}}, \quad i,j=1,2,3, \tag{4.2}$$

where $\mathbf{R}$ is the proper orthogonal tensor and R_{ij} are the components of the tensor $\mathbf{R}$ in the basis $\mathbf{e}_i$. Let m_i^{c} and m_i be the components of the magnetization vector in the bases $\mathbf{e}_i^{\mathrm{c}}$ and $\mathbf{e}_i$, respectively. They are related by $m_j^{\mathrm{c}} = R_{ij}m_i$. Further, let $\varepsilon_{ij}^{0^{\mathrm{c}}}$ and ε_{ij}^0 be the components of strain tensor $\boldsymbol{\varepsilon}^0$ in the bases $\mathbf{e}_i^{\mathrm{c}}$ and $\mathbf{e}_i$, respectively. The transformation rule for tensors in different bases yields $\varepsilon_{ij}^0 = R_{ip}\varepsilon_{pq}^{0^{\mathrm{c}}}R_{jq}$. It follows that

$$\begin{aligned}\frac{\partial\varepsilon_{ij}^0}{\partial m_k} &= R_{ip}R_{jq}\frac{\partial\varepsilon_{pq}^{0^{\mathrm{c}}}}{\partial m_k} = R_{ip}R_{jq}\frac{\partial\varepsilon_{pq}^{0^{\mathrm{c}}}}{\partial m_{\mathrm{s}}^{\mathrm{c}}}\frac{\partial m_{\mathrm{s}}^{\mathrm{c}}}{\partial m_k}\\ &= R_{ip}R_{jq}R_{ks}\frac{\partial\varepsilon_{pq}^{0^{\mathrm{c}}}}{\partial m_{\mathrm{s}}^{\mathrm{c}}},\end{aligned} \tag{4.3}$$

where the general expression of $\boldsymbol{\varepsilon}^0$ in terms of components of $\mathbf{m}$ in the crystal basis is given by (2.4) for cubic materials. Notice that summation over repeated indices is implied in (4.3) unless noted otherwise.

We next focus on calculating the stress $\boldsymbol{\sigma} = \mathbf{C}[\boldsymbol{\varepsilon} - \boldsymbol{\varepsilon}^0(\mathbf{m})]$ obtained by solving the equilibrium equation $(2.7)_2$. In Section 3.3 we propose a dual set of equations (3.20) and (3.21) to calculate the displacement gradient and traction along an arbitrary contour s inside a body Ω in which the magnetostrain is assumed to be piecewise uniform. The first step is to calculate the boundary displacement gradient and traction by letting the contour s coincide with the boundary $\partial\Omega$. Let the boundary $\partial\Omega$ and subboundaries $\partial\Omega_i$, $i = 1,\ldots,B$, be approximated by N_1 and $N_2^{(i)}$ line segments over which the normal tractions and tangential displacement gradients are assumed to be constant. The resulting discretized equations of (3.20) and (3.21) with the midpoints of the line segments chosen as the collocation points are

$$\begin{aligned}&\sum_{k=1}^{N_1}(\mathbf{W}^*)_{jk}(\mathbf{d}_{\mathbf{l}})_k\\ &\quad= \sum_{k=1}^{N_1}(\mathbf{U}^*)_{jk}(\mathbf{t}_{\mathbf{n}})_k + \sum_{p=1}^{B}\sum_{q=1}^{N_2^{(p)}}(\mathbf{U}^*)_{jq}(\mathbf{t}_{\mathbf{n}}^0)_q^p,\\ &\quad j = 1,2,\ldots,N_1,\end{aligned} \tag{4.4}$$

$$\begin{aligned}&\sum_{k=1}^{N_1}(\mathbf{W}^{*\mathrm{T}})_{jk}(\mathbf{t}_{\mathbf{n}})_k\\ &\quad= \sum_{k=1}^{N_1}(\mathbf{V}^*)_{jk}(\mathbf{d}_{\mathbf{l}})_k - \sum_{p=1}^{B}\sum_{q=1}^{N_2^{(p)}}(\mathbf{W}^{*\mathrm{T}})_{jq}(\mathbf{t}_{\mathbf{n}}^0)_q^p,\\ &\quad j = 1,2,\ldots,N_1,\end{aligned} \tag{4.5}$$

where $(\mathbf{d}_\mathbf{l})_k$ and $(\mathbf{t}_\mathbf{n})_k$ are the tangential displacement gradients and normal tractions at the kth element and the elements are numbered consecutively along the tangential direction $\mathbf{l}$ of the boundary $\partial\Omega$, and $(\mathbf{t}^0_\mathbf{n})^p_q = [(\mathbf{C}\boldsymbol{\varepsilon}^0)\mathbf{n}]^p_q$ are the normal tractions at the qth element of the subboundary $\partial\Omega_p$. If $j \neq k$, the matrices $\mathbf{U}^*$, $\mathbf{W}^*$ and $\mathbf{V}^*$ for anisotropic materials are given by the following analytic expressions:

$$\begin{aligned}(\mathbf{U}^*)_{jk} &= \Re[\mathbf{A}(\mathbf{G}^*)_{jk}\mathbf{A}^{\mathrm{T}}],\\ (\mathbf{W}^*)_{jk} &= \Re[\mathbf{A}(\mathbf{G}^*)_{jk}\mathbf{B}^{\mathrm{T}}],\\ (\mathbf{V}^*)_{jk} &= \Re[\mathbf{B}(\mathbf{G}^*)_{jk}\mathbf{B}^{\mathrm{T}}],\end{aligned} \tag{4.6}$$

where $(\mathbf{G}^*)_{jk} = \mathrm{Diag}\,[\delta^1_{jk}, \delta^2_{jk}, \delta^3_{jk}]$ are diagonal matrices with δ^1_{jk}, δ^2_{jk} and δ^3_{jk} given by

$$\begin{aligned}\delta^1_{jk} &= \frac{-1}{\mathrm{i}\pi}\frac{\hat{\zeta}^{(j)}_1}{\hat{\zeta}^{(k)}_1}\ln\left(\frac{\zeta^{(j+\frac{1}{2})}_1 - \zeta^{(k+1)}_1}{\zeta^{(j+\frac{1}{2})}_1 - \zeta^{(k)}_1}\right),\\ \delta^2_{jk} &= \frac{-1}{\mathrm{i}\pi}\frac{\hat{\zeta}^{(j)}_2}{\hat{\zeta}^{(k)}_2}\ln\left(\frac{\zeta^{(j+\frac{1}{2})}_2 - \zeta^{(k+1)}_2}{\zeta^{(j+\frac{1}{2})}_2 - \zeta^{(k)}_2}\right),\\ \delta^3_{jk} &= \frac{-1}{\mathrm{i}\pi}\frac{\hat{\zeta}^{(j)}_3}{\hat{\zeta}^{(k)}_3}\ln\left(\frac{\zeta^{(j+\frac{1}{2})}_3 - \zeta^{(k+1)}_3}{\zeta^{(j+\frac{1}{2})}_3 - \zeta^{(k)}_3}\right).\end{aligned} \tag{4.7}$$

Above in (4.7) $\hat{\zeta}^{(j)}_\alpha = \cos\theta_j + p_\alpha \sin\theta_j$ with θ_j being the angle between the jth element and the x_1-axis, $\zeta^{(k)}_\alpha = \xi^{(k)}_1 + p_\alpha\xi^{(k)}_2$ with $(\xi^{(k)}_1, \xi^{(k)}_2)$ and $(\xi^{(k+1)}_1, \xi^{(k+1)}_2)$ as the end points of the kth element, $\zeta^{(j+\frac{1}{2})}_\alpha = \xi^{(j+\frac{1}{2})}_1 + p_\alpha\xi^{(j+\frac{1}{2})}_2$ and $(\xi^{(j+\frac{1}{2})}_1, \xi^{(j+\frac{1}{2})}_2)$ is the midpoint of the jth element (see Fig. 3 for the detailed notation). If the closure of subdomain Ω_p is completely contained in Ω, the matrices $(\mathbf{U}^*)_{jq}$ and $(\mathbf{W}^*)_{jq}$ for anisotropic materials are the same as those in (4.6) except $\hat{\zeta}^{(q)}_\alpha$ and $\zeta^{(q)}_\alpha$ denote points in the qth element of subboundary $\partial\Omega_p$. On the other hand, for $j = k$ or if some parts of the subboundaries $\partial\Omega_p$ coincides with the boundary $\partial\Omega$ (and $j = q$ in this case),

$$\begin{aligned}(\mathbf{U}^*)_{jj} &= (\mathbf{V}^*)_{jj} = \mathbf{0},\\ (\mathbf{W}^*)_{jj} &= \frac{1}{2}\mathbf{I} \quad \text{(no sum over } j\text{)}.\end{aligned} \tag{4.8}$$

Finally, if the elastic material is isotropic, the explicit expression of these three matrices $\mathbf{U}^*$, $\mathbf{W}^*$ and $\mathbf{V}^*$ can be found in Wu et al. (1992).

Either (4.4) and (4.5), which are referred to as type 1 and type 2 equations, can be used to solve unknown boundary variables numerically. Once all the boundary data including $\mathbf{d}_\mathbf{l}$ and $\mathbf{t}_\mathbf{n}$ are obtained, we can use (3.20) and (3.21) together with (4.6) and (4.7) to calculate the stress at any points inside Ω. Examples to show the applicability of the formalism given by (4.4) and (4.5) are given in Appendix A.

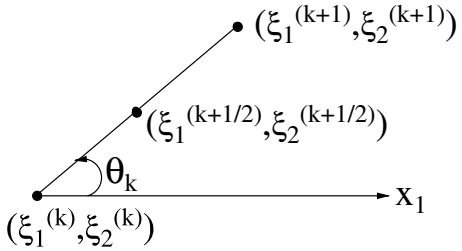

Fig. 3. Notation for the kth boundary element.

5. Results

In this section we explore the effect of intrinsic stress on the equilibrium magnetic domains and hysteresis calculated using the constrained approach. We also compare our results with those obtained based on the relaxed approach (i.e., the negligence of the influence of internal stress). We use Ni and Terfenol-D as the representative materials.

5.1. Extremely small magnetostriction

Ni is one of the common ferromagnetic materials with 10^{-5} order of magnitude of spontaneous magnetostriction. The associated magnetic material parameters are $M_s = 4.8 \times 10^5$ A/m, $A = 9 \times 10^{-12}$ J/m, $K^c_1 = -5.7 \times 10^3$ J/m^3, and $\lambda_{100} = -4.6 \times 10^{-5}$, $\lambda_{111} = -2.4 \times 10^{-5}$. The cubic anisotropic elastic constants in the crystal basis are $C_{11} = 2.5 \times 10^{11}$ N/m^2, $C_{12} = 1.6 \times 10^{11}$ N/m^2, $C_{66} = 1.18 \times 10^{11}$ N/m^2 in terms of Voigt notation.

We consider a single crystal Ni film with 100 nm$\times$100 nm$\times$10 nm dimensions. Assume the crystal basis coincides with the reference basis. There are no external stress and applied field, and

therefore, $\boldsymbol{\sigma}^* = \mathbf{0}$ and $\mathbf{H}^0 = \mathbf{0}$ in this case. The initial magnetization is $\mathbf{m}(\mathbf{x}) = \mathbf{e}_2$ and the final results of magnetization evolution described by LLG equation are shown in Fig. 4(a) and (b) under the condition $|\mathbf{m} \times \mathbf{h}^{\text{eff}}| < \epsilon$ where $\epsilon = 10^{-4}$ and $\mathbf{h}^{\text{eff}} = \frac{1}{M_s}\mathbf{H}^{\text{eff}}$. We have also used the smaller parameter $\epsilon = 10^{-5}$ as the criterion and found that the results are almost the same as those obtained using the original criterion. Note that Fig. 4(a) and (b) are magnetization patterns obtained using the relaxed and constrained approach. Obviously the results show that there are no significant differences between these two methods; in other words, the effect of intrinsic stress on magnetic domain patterns is not significant for magnetostrictive materials with extremely small magnetostriction.

We next investigate the hysteresis property such as coercivity of Ni thin films under intrinsic stress. The external field $\mathbf{H}^0$ is applied along the $\mathbf{e}_2$ direction with cycling magnitudes. Fig. 5(a) shows the simulated hysteresis loops calculated based on the relaxed (dashed line) and constrained (continuous line) approaches. The overall loops appear to be similar while there is a difference in coercive fields. Let H_c^r and H_c^c be the coercive magnetic fields obtained by relaxed and constrained methods. According to Fig. 5(a) $H_c^r = 7160$ A/m and $H_c^c = 8750$ A/m. The error estimate is

$$\frac{|H_c^r - H_c^c|}{H_c^c} \times 100 \approx 18\%.$$

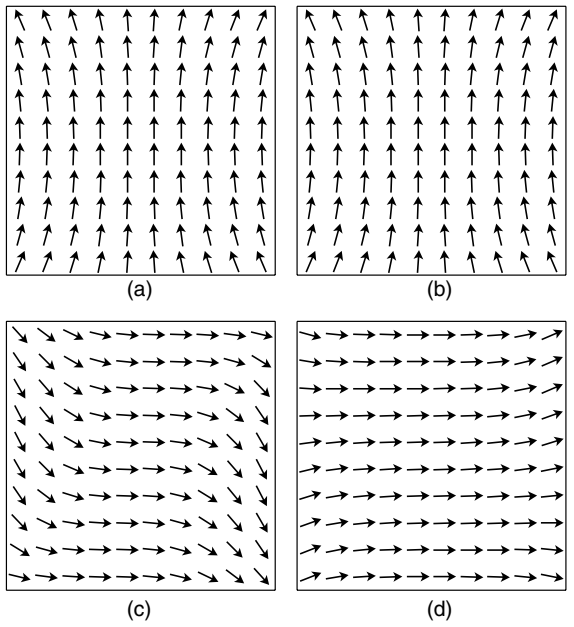

Fig. 4. Magnetic domain patterns for Ni films simulated based on the relaxed (a) and constrained (b) approaches. Magnetic domain patterns for Terfenol-D films simulated based on the relaxed (c) and constrained (d) approaches.

It is expected that H_c^c is larger than H_c^r since more energy input is needed to overcome the increase of elastic energy due to incompatible magnetostrain during magnetization rotation against reversal magnetic field.

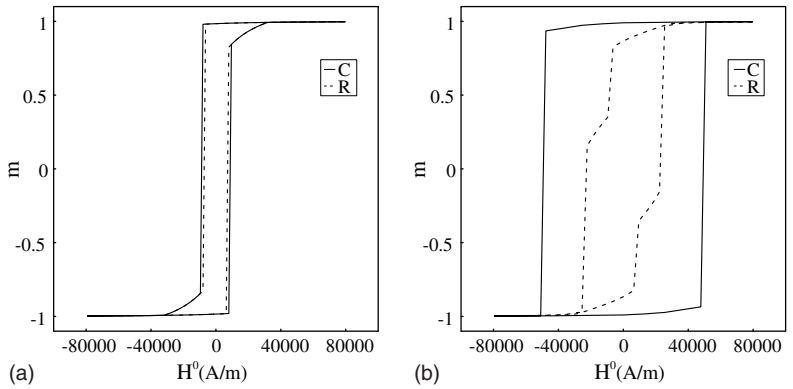

Fig. 5. Hysteresis loops calculated based on the constrained (C) and relaxed (R) approaches: (a) Ni thin films; (b) Terfenol-D thin films.

5.2. Large magnetostriction

Terfenol-D ($Tb_xDy_{1-x}Fe_2$, $x \approx 0.3$) is one of giant magnetostrictive materials with 10^{-3} order of magnitude of magnetostriction. The relevant magnetic properties of Terfenol-D are $M_s = 8\times10^5$ A/m, $A = 9 \times 10^{-12}$ J/m, $K_1^c = -6 \times 10^4$ J/m^3, and $\lambda_{100} \approx 0$, $\lambda_{111} = 1.64 \times 10^{-3}$ (Clark, 1986; Lord and Harvey, 1994). The bulk cubic elastic constants in the crystal basis are $C_{11} = 1.41 \times 10^{11}$ N/m^2, $C_{12} = 6.48 \times 10^{10}$ N/m^2 and $C_{66} = 4.87 \times 10^{10}$ N/m^2 in terms of Voigt notation (Dewar, 1997).

5.2.1. Uniform magnetization

Consider a single crystal Terfenol-D thin film with 100 nm×100 nm×10 nm dimensions. The crystal orientation is assumed to be $[\bar{1}\,\bar{1}\,1]_c||\mathbf{e}_1$ and $[1\,1\,2]_c||\mathbf{e}_2$ as shown in Fig. 6(a). There are no applied traction and field in this case; therefore, we take $\boldsymbol{\sigma}^* = \mathbf{0}$ and $\mathbf{H}^0 = \mathbf{0}$ in (2.13). The initial magnetization pattern is $\mathbf{m} = \mathbf{e}_1$ and the final results of magnetization evolution described by LLG equation are shown in Fig. 4(c) and (d) under the same criterion described in the case of Ni. Note that Fig. 4(c) and (d) are magnetization patterns simulated using the relaxed and constrained approaches.

In contrast to the case of Ni films, results simulated based on these two methods are completely different as can be seen in Fig. 4(c) and (d). In the former case, the elastic energy is not taken into account due to the negligence of intrinsic stress. So magnetization vectors are free to rotate and prefer to be oriented in one of the easy axes. As $K_1^c < 0$, $\langle 1\,1\,1\rangle_c$ is the easy direction for Terfenol-D. However, only in-plane easy axes including $[\bar{1}\,\bar{1}\,1]_c$ and $[1\,1\,1]_c$ are taken into account since Gioia and James (1997) have shown that the in-plane magnetization is the preferred state for very thin ferromagnetic films to reduce demagnetization energy. Combining all these facts leads to domain patterns shown in Fig. 4(c): magnetization vectors are aligned to $[\bar{1}\,\bar{1}\,\bar{1}]_c$ direction on both right and left sides of the film because of reduction of the stay field energy, and to $[\bar{1}\,\bar{1}\,1]_c$ in the middle to reduce the anisotropy energy.

On the other hand, the elastic energy plays an important role in equilibrium domain patterns for magnetic materials with large magnetostriction. The consideration of intrinsic stress due to magnetization rotation and boundary conditions prevents magnetization vectors from deviating too much from their initial easy direction $[\bar{1}\,\bar{1}\,1]_c$ during evolution. As a result, most of magnetization vectors in Fig. 4(d) are oriented to $[\bar{1}\,\bar{1}\,1]_c$ while the rest of them on both right and left sides of the film deviate a little from the easy direction to reduce the stay field energy.

Finally we study hysteresis of Terfenol-D thin films. The external field $\mathbf{H}^0$ is applied along the $\mathbf{e}_1$ direction with cycling magnitudes. Fig. 5(b) shows the simulated hysteresis loops calculated based on

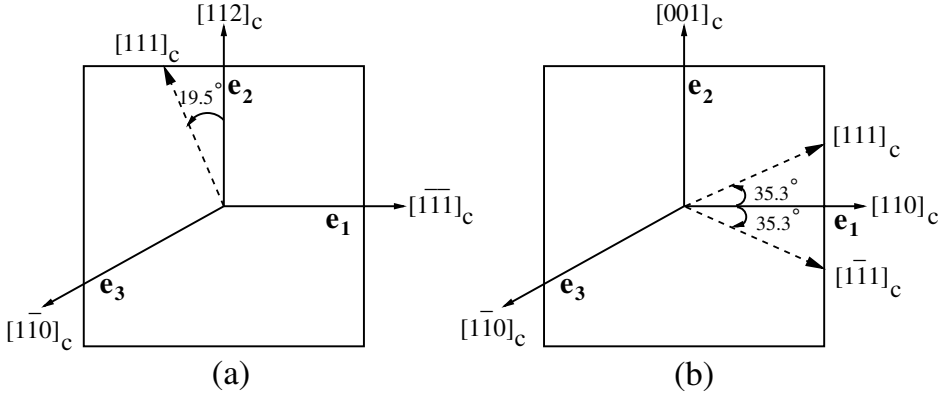

Fig. 6. Crystal orientations for single crystal Terfenol-D films with $\langle 1\,1\,1\rangle_c$ easy axes.

the relaxed (dashed line) and constrained (continuous line) approaches. In contrast to the results shown in Fig. 5(a) and (b) shows a wide difference in hysteresis loops simulated using these two distinct methods. Let H_c^r and H_c^c be the coercive magnetic fields obtained by relaxed and constrained approaches. According to Fig. 5(b) $H_c^r = 23{,}900$ A/m and $H_c^c = 49{,}300$ A/m, and the error estimate is

$$\frac{|H_c^r - H_c^c|}{H_c^c} \times 100 \approx 52\%.$$

In this case we have found that the coercive magnetic field H_c^c is twice larger than H_c^r obtained without consideration of intrinsic stress.

5.2.2. Twin

The magnetic domain patterns simulated in Section 5.2.1 are not commonly observed in Terfenol-D crystals at zero applied field. Instead, the observed microstructure is very complicated in the MFM image (Lord et al., 1997; Schmidt et al., 1998). Most of domain patterns appear in the way which we call "twins" (James and Kinderlehrer, 1993). We thus investigate the effect of intrinsic stress on this special microstructure.

Consider a single crystal Terfenol-D thin film with 200 nm × 200 nm × 10 nm dimensions. The crystal orientation is assumed to be $[1\,1\,0]_c || \mathbf{e}_1$ and $[0\,0\,1]_c || \mathbf{e}_2$ as shown in Fig. 6(b). Assume $\boldsymbol{\sigma}^* = \mathbf{0}$ and $\mathbf{H}^0 = \mathbf{0}$ in (2.13). There are two easy axes in the plane of the film: one is along $[1\,1\,1]_c$ and the other is along $[1\,1\,\bar{1}]_c$. The angle between the easy axis and $\mathbf{e}_1$ direction is about 35.3° as also shown in Fig. 6(b). The twinning plane is $(0\,0\,1)_c$ plane associated with the $[1\,1\,1]_c$ and $[\bar{1}\,\bar{1}\,1]$ magnetization pair. Let

$$\begin{aligned} \mathbf{m}_1 &= \frac{2}{\sqrt{6}}\mathbf{e}_1 + \frac{1}{\sqrt{3}}\mathbf{e}_2, \\ \mathbf{m}_2 &= -\frac{2}{\sqrt{6}}\mathbf{e}_1 + \frac{1}{\sqrt{3}}\mathbf{e}_2 \end{aligned} \tag{5.1}$$

be aligned to the easy directions $[1\,1\,1]_c$ and $[\bar{1}\,\bar{1}\,1]_c$, respectively. So the anisotropy energy is zero. From (2.4) and the crystal orientation shown in Fig. 6(b), the associated components of magnetostrain in the reference basis are

$$\begin{aligned} \boldsymbol{\varepsilon}^0(\mathbf{m}_1) &= \frac{\lambda_{111}}{2}\begin{pmatrix} 1 & \sqrt{2} & 0 \\ \sqrt{2} & 0 & 0 \\ 0 & 0 & -1 \end{pmatrix}, \\ \boldsymbol{\varepsilon}^0(\mathbf{m}_2) &= \frac{\lambda_{111}}{2}\begin{pmatrix} 1 & -\sqrt{2} & 0 \\ -\sqrt{2} & 0 & 0 \\ 0 & 0 & -1 \end{pmatrix}. \end{aligned} \tag{5.2}$$

Set $\hat{\mathbf{n}} = \mathbf{e}_2$. The condition $(\mathbf{m}_1 - \mathbf{m}_2) \cdot \hat{\mathbf{n}} = 0$ implies that there are no internal "magnetic charges" on the twin plane and the demagnetization energy is reduced to zero if the boundary effect is neglected. In addition, choosing $\mathbf{a} = \sqrt{2}\lambda_{111}\mathbf{e}_1$, we find $\boldsymbol{\varepsilon}^0(\mathbf{m}_1) - \boldsymbol{\varepsilon}^0(\mathbf{m}_2) = \mathbf{a} \otimes \mathbf{n} + \mathbf{n} \otimes \mathbf{a}$ satisfying the compatibility condition (Šilhavý, 1997). So $\boldsymbol{\varepsilon}^0(\mathbf{m}_1)$ and $\boldsymbol{\varepsilon}^0(\mathbf{m}_2)$ are compatible strain pair and, therefore, the intrinsic stress vanishes, so is elastic energy.

The initial magnetization pattern is $\mathbf{m} = \mathbf{m}_1$ for $0 < x_2 < 100$ nm and $\mathbf{m} = \mathbf{m}_2$ for 100 nm $< x_2 < 200$ nm. The inclusion of exchange energy and boundary effect gives the final magnetic domain patterns shown in Fig. 7(a) and (b) based on the relaxed and constrained methods. Note that we have found the identical simulation results for different initial configurations as long as the deviations of initial magnetization vectors from the easy directions are kept within 15°. In order to see the differences between these two methods, let θ^r and θ^c be the angles of the magnetization vectors from the x_1-axis in Fig. 7(a) and (b). Fig. 8(a) is the contour plot showing the error estimate based on the formula $\frac{|\theta^r - \theta^c|}{\theta^c} \times 100$. The maximum error estimate is up to 30% concentrated in the middle lower and upper parts of the film. However, this error estimate would be meaningless if θ^c is close to 90° since we can take $90° - \theta^c$ as another reference angle. To see this, Fig. 7(a) and (b) shows the significant differences in angles in the domain wall region on the left-hand side of the film. But such a change in magnetization angles cannot be reflected by the original error estimate shown in Fig. 8(a). Therefore, we define another error estimate based on the formula $\frac{|\theta^r - \theta^c|}{\max|\theta^r - \theta^c|} \times 100$, and the result is shown in Fig. 8(b). The new comparison diagram not only shows the trend of the error estimate but also reflects the change inside the wall region simulated by different approaches.

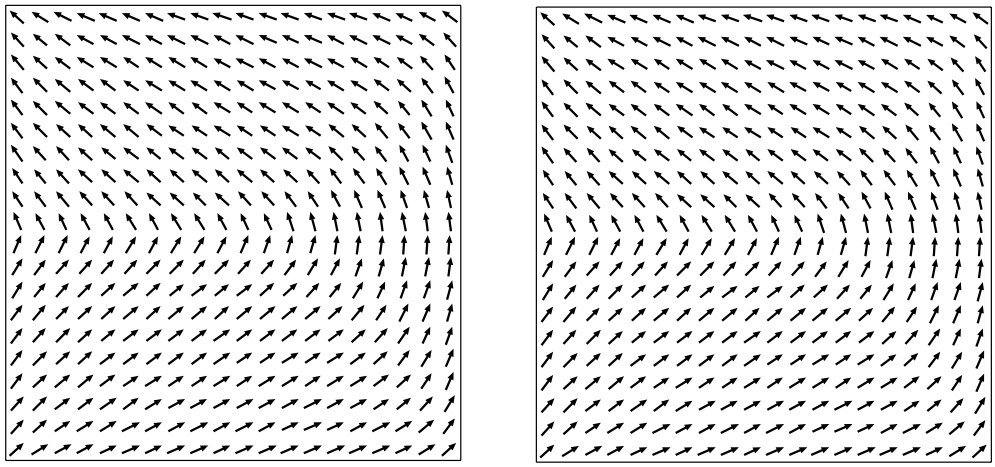

Fig. 7. Equilibrium twins for Terfenol-D films: (a) simulation based on the relaxed approach; (b) simulation based on the constrained approach.

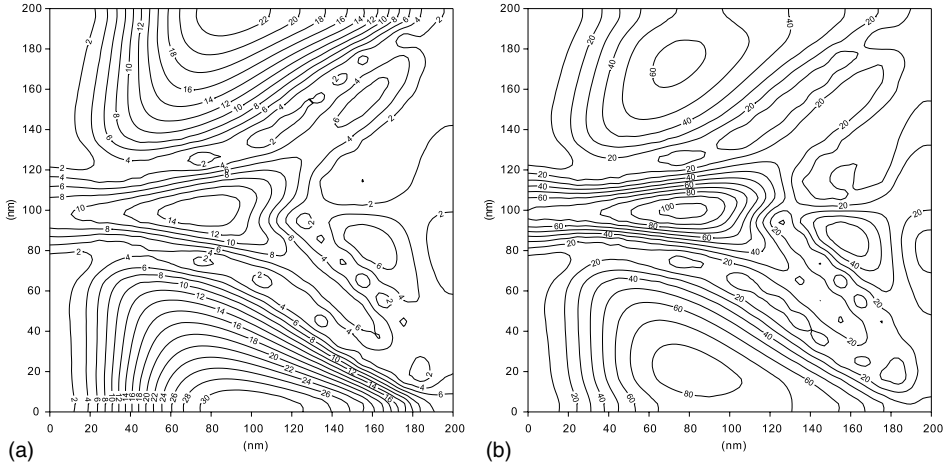

Fig. 8. (a) Error estimate for the twin structure based on the formula defined by $\frac{|\theta^f-\theta^c|}{\theta^c}\times 100$. (b) Error estimate for the twin structure based on the formula defined by $\frac{|\theta^f-\theta^c|}{\max|\theta^f-\theta^c|}\times 100$.

The average angle from the x_1-axis away from the domain wall region is around 30.9° in Fig. 7(a) while it is around 34.8° in Fig. 7(b). Clearly the magnetization vectors in Fig. 7(b) stay at much closer to the easy axes than those in Fig. 7(a) and it is also true inside the wall region. The negligence of elastic energy in Fig. 7(a) results in significant deviation from the easy directions for magnetization vectors near the boundary to reduce demagnetization energy. On the other hand, elastic energy becomes dominant in the case of large magnetostriction. The inclusion of elastic energy in Fig. 7(b) keeps magnetization vectors be aligned to the easy directions as close as possible at the cost of increase of stay field energy. This agrees with the ''constrained theory'' proposed by DeSimone and James (2002). In that theory the total energy is minimized over the special class of functions in

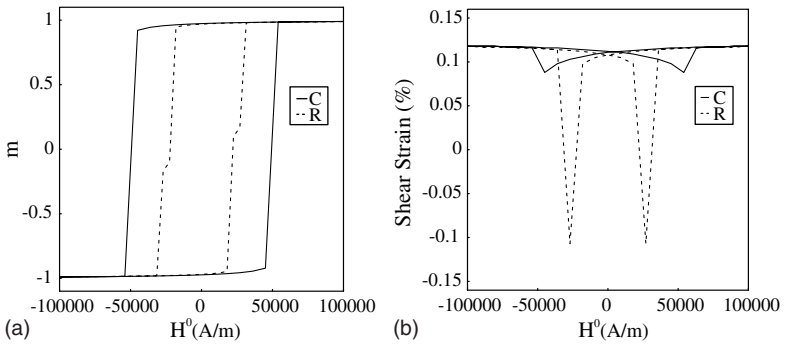

Fig. 9. (a) Hysteresis loops of average magnetization versus applied magnetic field calculated using the constrained (C) and relaxed (R) approaches. (b) Hysteresis loops of the average shear strain versus applied field simulated using the constrained (C) and relaxed (R) approaches.

which magnetization vectors are assumed to be oriented only along the easy directions. Our simulation confirms that this assumption turns out to be a reasonable approximation for materials with high anisotropy and large magnetostriction.

Finally, we investigate the hysteresis property. Let an external magnetic field be applied cyclically along the diagonal (45°) direction of this square film. The average magnetization projected on the diagonal direction versus applied field is shown in Fig. 9(a) calculated based on the relaxed (dashed line) and constrained (continuous line) approaches. Again we see the wide difference in the overall loops calculated based on these two methods. Fig. 9(b) shows the hysteresis of the average shear strain versus the applied magnetic field. The simulation based on the relaxed approach shows an intermediate step during the exchange of stability while this intermediate step disappears in the constrained approach. When the applied field decreases to zero from positive value, most of magnetization vectors are aligned to $[1\,1\,1]_c$ easy direction, resulting in positive shear strain as shown in Fig. 10(a). From (5.2) the angle due to shearing is about $\frac{\gamma}{2} = \mathbf{e}_2 \cdot \boldsymbol{\varepsilon}^0(\mathbf{m}_1)\mathbf{e}_1 = \frac{1}{\sqrt{2}}\lambda_{1\,1\,1} = 0.11\%$ for this Terfenol-D film. During the exchange of stability, the relaxed approach which neglects the intrinsic stress shows a stable intermediate step: most of magnetization vectors stay close to $[\bar{1}\,\bar{1}\,1]_c$ easy direction, causing the large negative shear strain as shown in Fig. 10(b). However, there is no such an intermediate step in the constrained approach. Instead, the magnetization is immediately rotated to $[\bar{1}\,\bar{1}\,\bar{1}]_c$ direction when the reversal applied field exceeds to coercive magnetic field as shown in Fig. 10(c). This gives rise to positive magnitude of shear again as magnetostrain $\boldsymbol{\varepsilon}^0(\mathbf{m})$ is an even function of magnetization (see (2.2)).

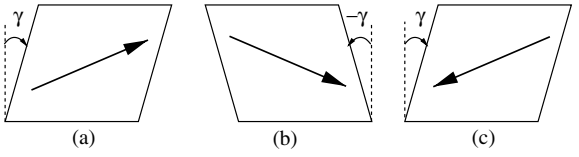

Fig. 10. The average shear deformation caused by magnetization rotation from (a) to (b) to (c). Note that magnetostrain $\boldsymbol{\varepsilon}^0(\mathbf{m})$ is an even function of magnetization $\mathbf{m}$.

6. Conclusion

We have explored the effect of intrinsic stress on the magnetostrictive behavior of ferromagnetic thin films. We start with a theoretical framework based on micromagnetics accounting in detail for the effect of stress. The micromagnetic formulation is a nonlocal, nonconvex variational problem subject to two constrained equations: Maxwell's and elastic equilibrium equations. The conventional approach which relaxes the elastic equilibrium equation takes into account only the external stress. The intrinsic stress caused by incompatible magnetostrain as magnetization rotates, however, is neglected by this method. In contrast, we

propose a modified boundary integral formalism to solve the elastic constrained equation. This formulation has the advantage of higher accuracy in the calculation of stress as well as faster rate of convergence than conventional displacement-based numerical schemes. We further implement it into the LLG solver to study both equilibrium and transient magnetization configurations.

We use Ni and Terfenol-D as the model materials. The former has small magnetostriction of the order of 10^{-5} while the latter has large magnetostriction of the order of 10^{-3}. Figs. 4 and 5 highlight the striking contrast in equilibrium magnetization and hysteresis calculated based on the constrained and relaxed methods. Our simulation shows that the relaxed approach turns out to be a reasonable approximation in predicting domain patterns and their evolution in the case of Ni films while it becomes a crude estimation for Terfenol-D films. In addition, we consider an example of twin which is the most observable microstructure in magnetostrictive materials. Fig. 8 shows the significant error estimate for the simulation of twins using the relaxed method. The result shows that away from the domain wall region the inclusion of magnetostrictive energy keeps magnetization vectors to be aligned to the easy axes as close as possible. This agrees with the "constrained theory" of DeSimone and James (2002) applied for materials with high anisotropy and large magnetostriction.

Acknowledgements

The authors are glad to acknowledge the financial support of the National Science Council of Taiwan under the grant NSC 90-2622-E-002-006.

Appendix A

We consider two examples to demonstrate the accuracy of the formalism given by (3.20) and (3.21). First we recall that the constitutive relation is $\boldsymbol{\sigma} = \mathbf{C}(\boldsymbol{\varepsilon} - \boldsymbol{\varepsilon}^0)$ where $\boldsymbol{\varepsilon}^0$ is the piecewise uniform eigenstain. A new kind of patch test of compatibility with geometry and boundary conditions is introduced in Fig. 11(a). The plane stress elastic constants used here are $C_{11} = 1.4767 \times 10^{11}$ N/m^2, $C_{12} = 0.5766 \times 10^{11}$ N/m^2, $C_{66} = 1.1848 \times 10^{11}$ N/m^2 in terms of Voigt notation. The eigenstrain is given by

$$\begin{aligned} \boldsymbol{\varepsilon}^0(\mathbf{x}) &= \boldsymbol{\varepsilon}_1^0 = \begin{pmatrix} 1 & 0 \\ 0 & 0 \end{pmatrix}, \quad \mathbf{x} \in \Omega_1, \\ \boldsymbol{\varepsilon}^0(\mathbf{x}) &= \boldsymbol{\varepsilon}_2^0 = \begin{pmatrix} 0 & 2 \\ 2 & 0 \end{pmatrix}, \quad \mathbf{x} \in \Omega_2. \end{aligned} \tag{A.1}$$

Note that one can check that $\boldsymbol{\varepsilon}_1^0$ and $\boldsymbol{\varepsilon}_2^0$ are compatible each other. So there is no internal stress across the boundary shared by $\partial\Omega_1$ and $\partial\Omega_2$. In fact, the exact solution is

$$\mathbf{u}(\mathbf{x}) = \begin{cases} (x_1, 0), & \mathbf{x} \in \Omega_1, \\ (0.05, 4x_1 - 0.2), & \mathbf{x} \in \Omega_2, \end{cases} \tag{A.2}$$

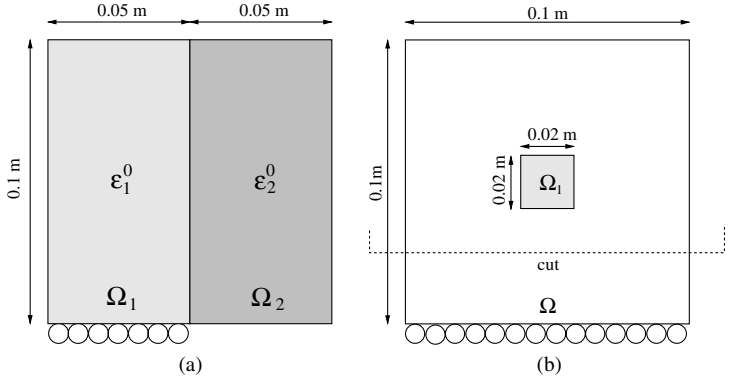

Fig. 11. (a) A patch test for strain compatibility. Note that the constrained boundary condition $u_2 = 0$ is enforced on the left-hand side of the bottom and is represented by circles. (b) A model problem to test the accuracy of the modified BEM formalism.

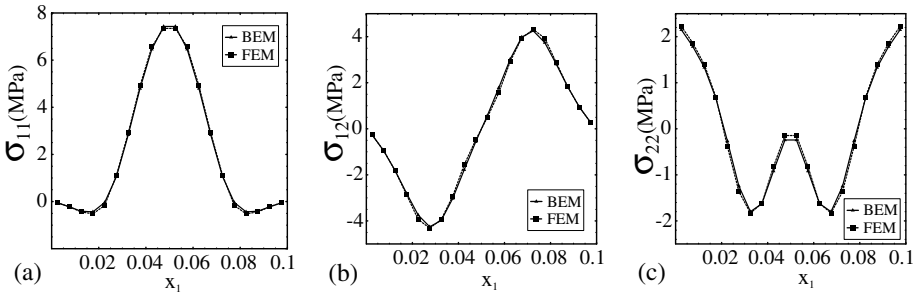

Fig. 12. Comparison of the modified BEM formulation with commercial NASTRAN FEM code for stresses computed along the line cut at 1/4 of the sideline of the body shown in Fig. 11(b).

which results in $\boldsymbol{\sigma} \equiv \mathbf{0}$. The computational result also shows that the computed stress $\boldsymbol{\sigma}$ is extremely close to zero which agrees with the exact solution. Finally, note that the total boundary elements used in the simulation are $N_1 = 6$, $N_2^{(1)} = 4$ and $N_2^{(2)} = 4$ where N_1 is the number of boundary elements on the whole boundary, $N_2^{(1)}$ and $N_2^{(2)}$ are the number of boundary elements used to describe the boundaries $\partial\Omega_1$ and $\partial\Omega_2$ (see (3.20) and (3.21)).

The next example with geometry and boundary conditions is shown in Fig. 11(b). The plane stress elastic constants used here are the same as those given in the previous example. The eigenstrain is given by

$$\boldsymbol{\varepsilon}^0(\mathbf{x}) = \begin{cases} \begin{pmatrix} 3.9 \times 10^{-4} & 0 \\ 0 & 3.9 \times 10^{-4} \end{pmatrix}, & \mathbf{x} \in \Omega_1, \\ \mathbf{0}, & \mathbf{x} \in \Omega \setminus \overline{\Omega}_1. \end{cases} \tag{A.3}$$

The total line elements used in the simulation are $N_1 = 80$ and $N_2^{(1)} = 16$ on the boundary $\partial\Omega$ and $\partial\Omega_1$, respectively. The stresses computed along the line cut at 1/4 of the sideline of the body are shown in Fig. 12. We also use the commercial NASTRAN FEM code to check the accuracy of the BEM formalism given by (3.20) and (3.21). Note that we have used the eight-node square mesh in the FEM simulation and the total number of meshes is 400. From Fig. 12 we find that the numerical results obtained by BEM simulation with few line elements on the boundaries agree well with those obtained by FEM simulation.

References

Aharoni, A., 1996. Introduction to the Theory of Ferromagnetism. Clarendon Press, Oxford.

Aharoni, A., Jakubovics, J.P., 1986. Cylindrical magnetic domains in small ferromagnetic spheres with uniaxial anisotropy. Philos. Mag. B 53, 133–145.

Berkov, D.V., Ramstöck, K., Hubert, A., 1993. Solving micromagnetic problems. Phys. Stat. Sol. (a) 137, 207–225.

Bhattacharya, K., 1993. Comparison of the geometrically nonlinear and linear theories of Martensitic transformation. Continuum Mech. Therm. 5, 205–242.

Brown, W.F., 1962. Magnetostatic Principles in Ferromagnetism. In: Wohlfarth, E.P. (Ed.), Selected Topics in Solid State Physics, vol. 1. North-Holland, Amsterdam.

Brown, W.F., 1963. Micromagnetics. Wiley, New York.

Brown, W.F., 1966. Magnetoelastic Interactions. Springer, Berlin.

Callegaro, L., Puppin, E., 1996. Stress dependence of coercivity in Ni films: thin films to bulk transition. Appl. Phys. Lett. 68, 1279–1281.

Callegaro, L., Puppin, E., 1997. Rotational hysteresis model for stressed ferromagnetic films. IEEE Trans. Magn. 33, 1007–1011.

Clark, A.E., 1980. In: Wohlfarth, E.P. (Ed.), Ferromagnetic Materials, vol. 1. North-Holland, Amsterdam (Chapter 7).

Clark, A.E., 1986. Magnetostriction in twinned [1 1 2] crystals of $Tb_{0.27}Dy_{0.73}Fe_2$. IEEE Trans. Magn. Mag-22, 973–975.

Crew, D.C., Lewis, L.H., 2001. Effect of grain alignment on magnetic structure in nanoscale material. IEEE Trans. Magn. 37, 2512–2514.

Cullen, J.R., Hathaway, K.B., Clark, A.E., 1997. Critical behavior of cubic magnetostrictive materials under stress. J. Appl. Phys. 81, 5417–5419.

Cullity, B.D., 1972. Introduction to Magnetic Materials. Addison-Wesley, Reading, MA.

Deng, H., Jarratt, J.D., Minor, M.K., Barnard, J.A., 1997. Artificially controlled stress anisotropy and magnetic properties of FeTaN thin films. J. Appl. Phys. 81, 4510–4512.

DeSimone, A., 1993. Energy minimizers for large ferromagnetic bodies. Arch. Rational Mech. Anal. 125, 99–143.

DeSimone, A., James, R.D., 2002. A constrained theory of magnetoelasticity. J. Mech. Phys. Solids 50, 283–320.

Dewar, G., 1997. Effect of the large magnetostriction of Terfenol-D on microwave transmission. J. Appl. Phys. 81, 5713–5715.

Donahue, M.J., 1998. A variational approach to exchange energy calculations in micromagnetics. J. Appl. Phys. 83, 6491–6493.

Donahue, M.J., 2000. OOMMF User's Guide 1.1b0.

Donahue, M.J., McMichael, R.D., 1997. Exchange energy representation in computational micromagnetics. Physical B 233, 272–278.

Dym, C.L., Shames, I.H., 1973. Solid Mechanics: a Variational Approach. McGraw-Hill, New York.

Eringen, A.C., Maugin, G.A., 1990. Electrodynamics of Continua I–II. Springer, New York.

Fabian, K., Heider, F., 1996. How to include magnetostriction in micromagnetic models of Ti-tanomagnetite grains. Geophys. Res. Lett. 23, 2839–2842.

Fidler, J., Schrefl, T., 2000. Micromagnetic modeling—the current state of the art. J. Phys. D: Appl. Phys. 33, R135–R156.

Gilbert, T.L., 1955. A Lagrangian formulation of gyromagnetic equation of the magnetic field. Phys. Rev. 100, 1243.

Gioia, G., James, R.D., 1997. Micromagnetics of very thin films. Proc. Roy. Soc. London A 453, 213–223.

Gurtin, M.E., 1972. The Linear Theory of Elasticity. In: Handbuch der Physik, vol. VIa/2. Springer, Berlin.

Hubert, A., Schäfer, R., 1998. Magnetic Domains: The Analysis of Magnetic Microstructures. Springer, Berlin.

Hutter, K., van de Ven, A.A.F., 1978. Field Matter Interactions in Thermoelastic Solids. Springer, Berlin.

Izawa, F., 1984. Theoretical study on stress-induced demagnetization in magnetic recording media. IEEE Trans. Magn. Mag-20, 523–528.

Jackson, J.D., 1962. Classical electrodynamics. Wiley, New York.

James, R.D., 2002. Configurational forces in magnetism with application to the dynamics of a small-scale ferromagnetic shape-memory cantilever. Continuum Mech. Therm. 14, 55–86.

James, R.D., Kinderlehrer, D., 1990. Frustration in ferromagnetic materials. Continuum Mech. Therm. 2, 215–239.

James, R.D., Kinderlehrer, D., 1993. Theory of magnetostriction with applications to $Tb_xDy_{1-x}Fe_2$. Philos. Mag. B 68, 237–274.

James, R.D., Wuttig, M., 1998. Magnetostriction of Martensite. Philos. Mag. A 77, 1273–1299.

Jeong, T.G., Bogy, D.B., 1995. Demagnetization due to inverse magnetization effects in longitudinal thin film media. IEEE Trans. Magn. 31, 1007–1995.

Jiles, D.C., 1994. The development of highly magnetostrictive rare earth-iron alloys. J. Phys. D: Appl. Phys. 21, 1–11.

Jiles, D.C., Atherton, D.L., 1984. Theory of the magnetisation process in ferromagnetics and its application to the magnetomechanical effects. J. Phys. D: Appl. Phys. 17, 1265–1281.

Kellogg, O.D., 1969. Foundations of Potential Theory. Springer, Berlin.

LaBonte, A.E., 1969. Two-dimensional Bloch-type domain walls in ferromagnetic films. J. Appl. Phys. 40, 2450–2458.

Landau, L.D., Lifshitz, E., 1935. On the theory of the dispersion of magnetic permeability in ferromagnetic bodies. Phys. Z. Sowjetunion 8, 153–169.

Li, J., Bhattacharya, K., in preparation.

Lord, D.G., Harvey, D., 1994. Anisotropy in twinned Terfenol-D crystals. J. Appl. Phys. 76, 7151–7153.

Lord, D.G., Holden, A.P., Grundy, P.J., 1997. Magnetic force microscopy of Terfenol-D fracture surface. J. Appl. Phys. 81, 5728–5730.

Maugin, G.A., 1988. Continuum Mechanics of Electromagnetic Solids. North-Holland, Amsterdam.

Miltat, J., Thiaville, A., Trouilloud, P., 1989. Neel line structures and energies in uniaxial ferromagnetics with quality factor $Q > 1$. J. Magn. Magn. Mater. 82, 297–308.

Nakatani, Y., Uesaka, Y., Hayashi, N., 1989. Direct solution of the Landau–Lifshitz–Gilbert equation for micromagnetics. Jpn. J. Appl. Phys. 28, 2485–2507.

Oden, J.T., Reddy, J.N., 1976. An Introduction to the Mathematical Theory of Finite Elements. Wiley, New York.

Pao, Y.H., Yeh, C.H., 1973. A linear theory for soft ferromagnetic elastic solids. Int. J. Eng. Sci. 11, 415–436.

Podio-Guidugli, P., 2001. On dissipation mechanism in micromagnetics. Eur. Phys. J. B 19, 417–424.

Ross, C.A., Schabes, M.E., Ranjan, R., Bertero, G., Chen, T., 1996. The role of stress-induced anisotropy in longitudinal thin film magnetic recording media. J. Appl. Phys. 79, 5342–5344.

Schmidt, J., Tickle, R., Skidmore, G.D., Merton, C., James, R.D., Dahlberg, E.D., 1998. Microscopic stress-induced magnetization changes in a fracture (1 1 1) surface of Terfenol-D observed with magnetic force microscopy. J. Magn. Magn. Mater. 190, 98–107.

Šilhavý, M., 1997. The Mechanics and Thermodynamics of Continuous Media. Springer, Berlin.

Shu, Y.C., 2002. Strain relaxation in an alloy film with a rough free surface. J. Elasticity 66, 63–92.

Shu, Y.C., Bhattacharya, K., 2001. Domain patterns and macroscopic behavior of ferroelectric materials. Philos. Mag. B 81, 2021–2054.

Stroh, A.N., 1958. Dislocations and cracks in anisotropic elasticity. Philos. Mag. 7, 625–646.

Thiaville, A., Garcia, J.M., Miltat, J., 2002. Domain wall dynamics in nanowires. J. Magn. Magn. Mater. 242–245, 1061–1063.

Tickle, R., James, R.D., 1999. Magnetic and magnetomechanical properties of Ni_2MnGa. J. Magn. Magn. Mater. 195, 627–638.

Tiersten, H.F., 1965. Variational principle for saturated magnetoelastic insulators. J. Math. Phys. 6, 779–787.

Ting, T.C.T., 1996. Anisotropic Elasticity—Theory and Application. Oxford University Press, New York.

Ullakko, K., Huang, J.K., Kantner, C., O'Handley, R.C., Kororin, V.V., 1996. Large magnetic-field-induced strains in Ni_2MnGa single crystals. Appl. Phys. Lett. 69, 1966–1968.

Voltairas, P.A., Fotiadis, D.I., Massalas, C.V., 2000a. Magnetization reversal in thin ferromagnetic films under mechanical stress. Int. J. Eng. Sci. 38, 903–919.

Voltairas, P.A., Fotiadis, D.I., Massalas, C.V., 2000b. Non-uniform magnetization reversal in stressed thin ferromagnetic films. J. Magn. Magn. Mater. 213, 43–50.

Wu, G.H., Wang, W.H., Chen, J.L., Ao, L., Liu, Z.H., Zhan, W.S., 2002. Magnetic properties and shape memory of Fe-doped $Ni_{52}Mn_{24}Ga_{24}$ single crystals. Appl. Phys. Lett. 80, 634–636.

Wu, K.C., 2000. Nonsingular boundary integral equations for two-dimensional anisotropic elasticity. ASME J. Appl. Mech. 67, 618–621.

Wu, K.C., Chiu, Y.T., Hwu, Z.H., 1992. A new boundary integral equation formulation for linear elastic solids. ASME J. Appl. Mech. 59, 344–348.

Zhu, B., Lo, C.C.H., Lee, S.J., Jiles, D.C., 2001. Micromagnetic modeling of the effects of stress on magnetic properties. J. Appl. Phys. 89, 7009–7011.

Zhu, J.G., 1993. Transition noise properties in longitudinal thin film media. IEEE Trans. Magn. 29, 195–200.